Materials Chemistry Today, Volume 17, September 2020, Article number 100304
DOI:10.1016/j.mtchem.2020.100304

Functional Nanocomposites for Energy Storage: Chemistry and New Horizons

Shuyang Chen[1], Alex Skordos[1*], Vijay Kumar Thakur [1,2,3*]

[1]Enhanced Composites and Structures Center, School of Aerospace, Transport and Manufacturing, Cranfield University, Bedfordshire MK43 0AL, UK

[2]Biorefining and Advanced Materials Research Center, Scotland's Rural College (SRUC), Kings Buildings, Edinburgh, EH9 3JG, UK

[3]Department of Mechanical Engineering, School of Engineering, Shiv Nadar University, Uttar Pradesh 201314, India

*Corresponding authors: a.a.skordos@cranfield.ac.uk; Vijay.Thakur@sruc.ac.uk

Abstract

Energy storage devices are one of the hot spots in recent years due to the environmental problems caused by the large consumption of unsustainable energy such as petroleum or coal. Capacitors are a common device for energy storage, especially electrical energy. A variety of types including electrolytic capacitors, mica capacitors, paper capacitors, ceramic capacitors, film capacitors, and non-polarized capacitors have been proposed. Their specific applications depend on their intrinsic properties. Dielectric capacitors have reasonable energy storage density, with current research focusing on the enhancement of energy density and making the materials more flexible as well as lightweight. Improvement strategies are based on the premise that use of two or more different materials (e.g. polymers and ceramics/metals) at an optimal formulation can result in properties that combine the advantages of the precursor materials. Different polymers especially fluoropolymers (e.g. PVDF and PVDF based co-polymer) are the main components in dielectric nanocomposites for capacitors with high energy storage performance. In this article, we have briefly summarized the recent advances in functional polymers nanocomposites for energy storage applications with a primary focus on polymers, surface engineering, functional groups and novel synthesis/ manufacturing concepts applied to new materials. The article presents a unique integrated structure and approaches providing key knowledge for the design and development of novel, low-cost, multi-functional next-generation energy storage materials with improved efficiency.

Key Words: Polymers; Nanocomposites; Surface Engineering; Energy Storage; Chemistry

1. Introduction

The upsurge in the population and the growth of global economy increase energy consumption [1]. According to the data of the US Energy Information Administration [2] the main energy resources that the world relies on are unsustainable energy including petroleum, coal and natural gas and other types of non-environmentally friendly fossil fuels. Environmental issues such as excessive greenhouse gas emission are not the only problem that the large amount consumption of unsustainable energy can bring, as the price of fossil fuel can influence the global economy as well with the depletion of these resources becoming a critical issue in the future. Hence, the demand for sustainable and renewable forms of energy such as wind and solar power has significantly increased in recent years [1]. The idea of using renewable energy has been raised several decades ago. However, unsustainable energy is still the main type consumed to an extent due to the constraints related to the climate or geography [1]. Energy storage technologies can play a major role in overcoming some of these constraints to meet the demand for supply at the point of consumption, whilst allowing the production of energy at a different location [1].

Different types of energy storage devices are currently in use including capacitors, batteries, flywheels, superconducting magnetic energy storage (SMES) systems and solid oxide fuel cells (SOCF). **Figure 1** [2] illustrates the trade-off between specific energy and specific power of different types of devices. Among these devices, high energy density capacitors play a very important role with current applications such as Marx generators, pulsed laser, particle accelerators, and electromagnetic generation. Also, capacitors can meet high specifications including maintaining a high capacitance and small amount of energy losses even when the usage rate is above the average level [3]. Capacitors store electric charge when a voltage is applied in the circuit and release the charges into the circuit when necessary. They generally comprise two metallic usually planar electrodes and a dielectric plate between them. The metallic electrodes produce positive and negative charges when a voltage is applied, whilst the insulating dielectric material does not allow any electrical charges passing through resulting in storage through polarization. The insertion of the dielectric material can reduce the effective electric field required to generate a certain level of charge at the electrodes, therefore, improving the performance of the capacitor. One of the challenges is that the dielectric properties of the capacitor can degrade over time as the dielectric material is exposed to temperature changes, environmental degradation and changes at a material level due to the applied high voltage resulting in the reduction of efficiency and performance. Dielectric capacitors are used in several applications summarized in **Figure 2**.

Use of polymers as matrix and inorganic nanofillers as reinforcement has been proposed in both academic and industrial research on dielectric capacitors in the last decade [4]. Some popular nanofillers such as carbon nanotube (CNT), carbon black (CB) or metal oxides such as TiO_2 have been widely used due to their attractive mechanical and electrical properties [4]. The addition of nanofiller is extremely useful

to improve dielectric properties; however, a large amount of nanofillers in the host can cause problems such as aggregation leading to degradation of properties [4]. Different types of polymers have been used as hosts such as elastomers, thermosets or thermoplastics. Elastomers are most widely used as matrix; among elastomers, silicone rubber, natural rubber and butadiene rubber have been used [4].

Research on dielectric capacitors is not only focused on the material selection but also on modification since the interface between nanofillers and the polymer matrix is the key to obtain appropriate properties [4]. Traditional methods including dopant, surface modification and other techniques will be discussed in detail in this review. Kumar et al. [4] vulcanized silicone rubber at room temperature and used $BaTiO_3$ as nanofiller with CNT and CB fillers to test the energy harvesting ability of the material. The results showed that when the fraction of $BaTiO_3$ is 50 phr (parts per hundred rubber), the energy harvesting increases at all strains [4]. One of the problems of the rubbers or polymers is temperature resistance; dielectric materials or dielectric capacitors are often used for vehicles, oil and gas exploration, avionics or advanced propulsion systems, which are associated with a high temperature working environment [5]. A high-temperature working environment is challenging for the polymer, e.g. the working environment of hybrid electric vehicles is at temperatures higher than 140ºC, but the melting temperature of some polymers like BOPP is between 130 to 170ºC [5]. This means that the use of this type of material requires an extra active cooling system or redesign of the electronic devices [5]. The design of high-temperature dielectric materials is different to the design of room temperature dielectric materials; some additional factors need to be considered; e.g. thermal stability, dielectric breakdown, conduction mechanisms and relative permittivity and dissipation factor [5]. Li et al. [5] listed some current polymers that can work in high-temperature conditions, involving polyimide (PI) synthesized from dianhydride and diamine monomer by a condensation reaction and followed by chemical irradiation resulting in up to 500ºC working temperature or fluorene polyester (FPEs) and cross-linked divinyltertramethyldisiloxanebis (c-BCBs) prepared through the reaction between fluorene bisphenol and phthalic chloride [5]. These materials allow a working temperature of up to 330ºC [5]. Apart from the synthesis of a new polymer, the development of a polymer nanocomposite is another way to overcome temperature issue, e.g. adding inorganic dopants or producing sandwich structured composites [5].

2. Material related developments

2.1 Polymer-based capacitors

It is well-known that the performance of all the equipment needs support from materials; therefore, research related to the material selection based on functions of different devices has attracted much attention. Dielectric capacitors produced by dielectric polymers have many advantages like low manufacturing cost and small size [3]. Besides, the electric field applied to the electric circuit is determined by the energy

density of the materials used; the high breakdown strength of polymers means they can have higher charge storage capacity than ceramics or other materials [3]. Polymers can be classified into three broad types depending on their structure at chain level: (i) linear chain polymers which contain long and straight-chain, (ii) branched-chain polymers, which involve branches of the linear chains, and (iii) cross-linked polymers in which chains form a three-dimensional network [3,6–12]. In addition, polymers can also be classified into polar or non-polar based on their molecular groups [6]. Non-polar polymers usually have a lower dielectric constant because single dipole moments eliminate each other due to symmetry [6]. Non-polar polymers include low-density polyethylene (LDPE), polyolefins, polytetrafluoroethylene (PTFE) and others. In contrast to non-polar polymers, instead of cancelling each other, the dipoles of polar polymers are asymmetric and generally exhibit higher dielectric constant [6]. Conventional polymers for capacitors include polyester (PET), polycarbonate (PC) and biaxially oriented polypropylene (BOPP) [3]. Another usual way to classify polymers is into thermoplastics and thermosets [13]. Thermoplastic polymers have a linear structure and can be remolded when the temperature is above a certain level, the process is reversible; thermosetting polymers cannot be thermally re-processed and usually characterized by a cross-linking structure [13]. Typical examples of thermoplastics are polyolefins and polystyrene, while epoxy, unsaturated polyesters and phenol-formaldehyde resins are representative examples of thermosets [13].

Within all these materials, PVDF based ferroelectric polymers and co-polymers motivate a large amount of research due to their large permittivity and dielectric strength [7–12] and have also been widely used as conductive and flexible polymer electrolytes. Some characteristics of PVDF such as its extraordinary electrical resistance, mechanical strength, and high-volume resistivity, make it an appropriate material for the manufacture of dielectric devices for energy storage application [3]. Compared with other polymers, PVDF has higher dielectric constant and breakdown strength and as a result, it has better energy storage density [6]. There are many forms of PVDF including α, β and γ phases whilst transition from α to other forms can be enhanced by mechanical stretching (**Figure 3**). Although the α-phase is non-polar, the other two phases have high dielectric constants due to the presence of net dipole moment and high polarizability [14].

PVDF and PVDF-based co-polymers have also been reported to act as the host of gel polymer electrolytes because of their intrinsic favorable properties such as high breakdown strength and flexibility [15]. Gel polymer electrolytes are mixtures of solid polymer and liquid electrolytes, which can be used for drug and stem cell delivery. Ionic liquids have recently been used to replace conventional electrolytes due to their low ignitability and high thermal and electrochemical stability [15]. The selection of host polymer is important for gel electrolytes; different polymers can directly influence the final performance [15]. Das et al. [15] have reported that PVDF-HFP copolymers show better compatibility with the mobile phase and higher mechanical strength compared to other polymers like PAN, PVA and PMMA, which makes them an ideal choice. The crystalline structure of PVDF helps to maintain the mechanical strength whilst the amorphous structure of PHFP successfully traps liquid electrolytes [15]. This means

that the amorphous phase provides the backbone for the electrolyte and the crystalline phase remains relatively unaffected during the application, which implies that the crystalline phase maintains a significant part of its mechanical properties. If levels of crystallinity are significant, the crystalline phase can help the whole co-polymer to have a good mechanical performance and the resultant material might be softened but still has sufficient strength. These principles indicate that PVDF and PVDF based co-polymers could be the suitable for the matrix of composites, although, they still have some problems such as high remnant polarization and early saturation which results in poor energy density and low efficiency [16].

2.2. Nanocomposites based capacitors

The combination of different types of materials such as polymers and nanomaterials with different dimensions/structures to produce new types of capacitors has been extensively investigated, e.g. combination of graphene with perovskite ceramics [17]. Materials with high dielectric constant such as ceramics are highly desirable for use in the fabrication of capacitors. The use of ceramics as fillers to produce capacitors with better performance has been studied in thick film solutions [9]. Ezeigwe et al. [17] have reported the combination of zinc oxide with graphene to produce supercapacitors with improved energy and power density. Along with the use in dielectric capacitors, graphene is a good candidate for electrode applications because of its high electrical conductivity, high surface area to volume ratio, fast electron mobility, good thermal stability and flexibility [18–21]. A graphene/ZnO capacitor can reach energy and power density of 11.80Wh/kg and 42.48kW/kg respectively, which is significantly higher than the power and energy densities of pristine graphene showing that the metal oxide can improve the electrochemical properties of capacitors [17]. This is explained by the positive role of metal oxides in expanding the surface area of graphene and improving the capacitance by a redox reaction [18].

Despite their widespread use and high dielectric constant, perovskite ceramics have low dielectric and mechanical strength. Compared with ceramics, polymers are easy to process, flexible and exhibit low cost [12]. However, polymer has low permittivity and low energy storage density. Therefore, composite materials with the positive advantages of both ceramics and polymers have attracted much attention. Often, the properties of composites are not satisfactory due to the incompatibility between the ceramic filler and polymer matrix, which means that the polymer/ceramic nanocomposite needs further functionalization to improve the compatibility and the dielectric performance [22]. The selection of materials and their functionalization technique can significantly affect the electrical behavior and applications of the capacitors; therefore, most of the works on capacitors are related to the raw material modification, e.g. by doping, multi doping or surface functionalization [12].

Dielectric capacitors are normally categorized into ceramic- and polymer-based material [23]. Usually, PVDF or PVDF based co-polymers [6–8] are used as the matrix and ceramics such as ZnO [15-16] or TiO_2 [17] as reinforcement filler to produce nanocomposites. Compared with capacitors made by only ceramic or polymer,

composite dielectric capacitors have the advantages of easy processing, low manufacturing cost, flexibility, and lightweight [24]. Ceramics play a significant role in the enhancement of the dielectric properties of capacitors. Transition metal oxides with a cubic perovskite structure can also be used for actuators and transducers for the electronics industry and high-performance dielectrics due to their unique combination of optical, dielectric, electrostrictive and pyroelectric behavior [24]. Nanocrystalline oxides can be used to fabricate functional or intelligent materials by changing their electrical, magnetic, optical or chemical properties [25]. The use of nanomaterials brings additional benefits such as high sensitivity, quantum confinement and high surface to volume ratio [26]. Transition metal oxides and conducting polymers have been reported to provide 10~100 times better performance than electrical double-layer capacitors (e.g. carbon-based materials) because of their reversible and fast surface redox reaction [27]. Among the many possible metal oxides, including RuO_2 [28], NiO_2 [29] and MnO_2 [30], zinc oxide (ZnO) is one of the most appropriate electrode materials for capacitors because of the low cost, abundant availability, low environmental impact and electrochemical activity [31]. The energy density of zinc oxide is around 650 A/g, also, the exciton binding energy and bandgap of this material are unique at 60meV and 3.37eV respectively [32–34]. Das et al.[15] have investigated the combination of the PVDF based co-polymer (PVDF-HFP) with ZnO and TiO_2 separately. The TiO_2 based polymer electrolyte shows higher specific capacitance than ZnO due to the higher dielectric constant of TiO_2 which promotes ionic dissociation [15].

Barium titanium oxide (**Figure 4**) has also been used for different types of capacitors such as dielectric capacitors or multilayer ceramic capacitors due to its high permittivity and ferroelectric behavior. Barium titanium ($BaTiO_3$) has been successfully utilized to produce dielectric capacitors with excellent permittivity (K around 6000) and small grain size which is around 1 μm [35-36]. The synthesis procedure of the nanomaterials affects the electrical properties of the resulting composite [34]. The dielectric constant of $BaTiO_3$ can also be influenced by temperature. The dielectric constant has a peak value at the Curie point which is around 120ºC [18,37], which also indicates that the synthesis temperature could play the curial rule. The detail of how the working temperature affects the final properties is discussed in section 6.2. Modification through chemical additives has been attempted to reduce the Curie point to room temperature and achieve high permittivity at usual operating conditions [22]. The dielectric properties of capacitors produced by $BaTiO_3$ and polymer depend on grain size as well as on type and amount of doping [22]. Two mechanisms can be used to lower the Curie temperature of perovskite-type composites ($A^{2+}B^{4+}O^3$). The first mechanism is based on using chemical additives, or extra ions to substitute the original ions in the A^{2+}- or B^{4+}- sites and the second is using external pressure [38]. The first mechanism affects the unit cell size by adding ions with different radii to element A or B [38]. The second mechanism can control the unit cell size via biaxial or hydrostatic pressure [38]. The Curie temperature is determined by the microstructure of materials [39-40]. Hiroshima et al. [39] studied how the microstructure influences the Curie temperature in lead barium niobite solid solutions showing that shrunk grain sizes or lower pore density

and dilated grain boundaries can lead to the reduction of internal stress resulting in higher Curie temperature. Grain size is not the only governing factor; the diffusion of foreign ions in the matrix can also be a key parameter for the control of the Curie temperature of ferroelectric materials [38].

3. Modelling

All the modifications aim to produce dielectric capacitors with higher energy storage density [24]. The energy density (Ue) of dielectric capacitors can be calculated as follows [24]:

$$U_e = \int_{D_{max}}^{0} E dD \quad (1)$$

$$U_e = \varepsilon_0 \varepsilon_{eff} E_b^2 / 2 \quad (2)$$

where D is the electric displacement of dielectric materials, E represents the applied field which is restricted by the breakdown strength [24]. Equation (1) can be reduced to Equation (2), with ε_{eff} the effective permittivity and E_b the breakdown strength [41]. The electric displacement D is determined by the applied electric field which can is shown in the following expression [16]:

$$D = \varepsilon_0 \varepsilon_r E \qquad (3)$$

where ε_0= 8.85×10^{-12} Fm^{-1} is the vacuum permittivity, ε_r is the dielectric constant which is also known as relative dielectric permittivity. Generally, the dielectric constant for a linear dielectric is independent of the applied electric field, and results in the following expression [16]:

$$U_e = \frac{1}{2} \varepsilon_0 \varepsilon_r E^2 \qquad (4)$$

The effective permittivity, ε_{eff}, can be approximated by [42]:

$$\varepsilon_{eff} = \frac{\varepsilon_h f_h + \varepsilon_f f_f (\frac{E_f}{E_h})}{f_h + f_f (\frac{E_f}{E_h})} \qquad (3)$$

where $\varepsilon_{h,} f_h$ and ε_f, f_f are the volume fraction and permittivity of the matrix and filler respectively and E_f ,E_h the electric fields in the two components [42].

The Maxwell Garnet equation, Lichtenecker logarithmic formula and Bruggeman Self-Consistent Effective Medium model [6] have presented adequate approximations of the dielectric properties of composites up to a filler volume fraction of 20%. [43] Jayasundere and Smith (JS) investigated an improved Kerner model [44]:

$$\varepsilon_{eff} = \frac{\varepsilon_h f_h + \varepsilon_f f_f (A)(B)}{f_h + f_f (A)(B)} \qquad (4)$$

where

$$A = \frac{3\varepsilon_h}{\varepsilon_f + 2\varepsilon_h} \quad (5)$$

and

$$B = 1 + \frac{3f_f(\varepsilon_f - \varepsilon_h)}{\varepsilon_f + 2\varepsilon_h} \quad (6)$$

Alternatively, the breakdown strength and effective permittivity can be estimated even for a wider range of volume fractions by using the self-consistent effective medium theory (SC-EMT) [7]. The application of SC-EMT can simulate the interaction of particles with each other and with air voids [7]. This model can be used to represent the effect of adding fillers into a matrix with contrasting properties constant and reproduces localized hot spots generated by the field concentration in the filler [7]. The effective permittivity can be calculated as:

$$\varepsilon_{eff} = \varepsilon_1 + f_2(\varepsilon_2 - \varepsilon_1)a_2 + f_3(\varepsilon_3 - \varepsilon_1)a_3 \qquad (7)$$

Subscripts 1,2, and 3 represent the matrix, filler and voids respectively and a_r is the electric field concentration factors in each phase r [7]. The electric field concentration factor and applied electric field E_0 can be used to obtain the average electric field in each phase as $E_r = a_r E_0$ [7].

A calculation of a_r can be carried out as follows [7]:

$$a_r = 1 - s[(\varepsilon_r - \varepsilon_{eff})^{-1}\varepsilon_{eff} + s]^{-1} \quad r = 2,3 \qquad (8)$$

where s is the depolarization factor. The field concentration factor of the matrix can be expressed by the normalization condition [7]:

$$\sum_{r=1}^{3} f_r\, a_r = 1. \qquad (9)$$

Using equation 8, equation 9 can be solved to obtain a self-consistent effective permittivity [38].

4. Dielectric capacitors

The main role of dielectric capacitors or dielectric materials is acting as part of the electrical equipment [6]. They can be used for pulsed-power applications such as in radars, other applications including communication and video equipment [6]. Most electronic equipment, mobile phones or computers can benefit from the use of dielectric capacitors since instant energy uptake and delivery become possible. Furthermore, dielectric capacitors can also be applied to defense systems and high-frequency filtering. In addition, they can provide better performance for the vehicle, e.g. capacitors can provide much higher power than the continuous power associated with fuel cells, generators or batteries when the vehicle is under high power working conditions [45]. The power and energy densities are the two most important metrics used to assess the quality of energy storage devices. Whittingham et al. [46] compared the power density of different energy storage devices (**Figure 5)** including batteries, fuel cells, pseudocapacitors, electrostatic capacitors, internal combustion engines, and double-layer capacitors. The comparison shows that electrostatic capacitors have the highest

power density between ~104 and ~107 W/Kg but they also have the lowest energy density (0.001-0.1 Wh/Kg) [46].

The conventional fabrication process of dielectric polymer/ceramic nanocomposite materials including roll coating, hot pressing, drop-casting or spin-coating are now considered to be ineffective [47]. Yang et al. [47] reported a new way to print nanocomposites into three dimensional (3D) capacitors by projection-based stereolithography (SLA). It is an easy process, with high efficiency and low-cost 3D which has been used to manufacture engineering products and high fidelity patterns [48]. The usual procedure of the SLA method involves exposure of the photocurable liquid or polymer composite material regions under the light to generate cross-links followed layer by layer processing whilst computer-aided design (CAD) is needed to program the actual pattern [47]. The strategy of Yang et al. [47] was based on the use of polymer nanocomposite with PZT as filler; before application, the filler was mixed with Flex resins and ultrasonicated. An integrated tape-casting system was used by Yang et al. [47] to recoat thick layers on a transparent glass substrate to create uniform thin layers with a lower thickness which was recoated by moving the platform so that a reasonable gap between the cured layer and the glass substrate can be formed. Mask images were projected upwards onto the bottom of the substrate after the layer was recoated, and a two-channel sliding design was applied to ensure the newly cured layer is separated from the substrate. The design of two-channel sliding is based on the idea of controlling the shear force between the cured layer and the coated film [47]. Apart from Yang et al. [47], another novel 3D method to print dielectric polymers was investigated by Gonzalez et al. [49] using fused deposition modeling (FDM). In this method, a plastic filament is fed into a heated extruder and then laid down following a predetermined pattern dictated by the desired structure [49]. This type of 3D printing allows multiple printing at the same time, which means that it is possible to print the electrodes and the dielectric film at the same time [49].

In addition, dielectric capacitors can also be used in medical devices; one of the most well-known examples is defibrillators [6]. **Figure 6** is a simple schematic of a defibrillator [50]. Along with energy storage and harvesting, polymer-based nanocomposites have a wide range of applications. Moreover, dielectric capacitors can separate DC from AC, and used to store digital and analogue data. Besides, nano-composites are easy to synthesize, small in size, lightweight, low cost, and environmentally friendly [6]. In recent years, a large number of works related to the nanocomposites have been reported due to their wide application areas and industrial value.

5. Methods used to enhance dielectric properties

The combination of polymers - especially PP/ PVDF - and ceramic fillers with high dielectric constant has been identified as a very useful method to formulate high energy storage densities nanocomposites [15-17]. Polymers act as the matrix and either ceramic particles, fibers or 2D sheets can be used as fillers [51]. The large energy

density that dielectric capacitors can accommodate usually requires electric fields over 600 KV/mm, which is relatively high, limiting their applications in low voltage conditions and increasing the risk of failure during operation [52]. A number of works in the past few decades have proved that ceramic fillers can improve the energy density of polymer nanocomposites as well as their dielectric breakdown strength [47]. The highest electric field that can be applied to a dielectric capacitor is determined by its breakdown strength, whilst excessive electric field can cause irreversible damage like and the energy storage capability of capacitors for the charge and discharge cycle parameter [16]. The energy density of a capacitor is quadratically related to its breakdown strength for a linear dielectric [16]. The increase of breakdown strength is important during the design of a new dielectric nanocomposite, otherwise, increased the dielectric constant or efficiency is meaningless [16].

5.1 Dopant addition and surface modification

Theoretically, adding $BaTiO_3$ or other ferroelectric ceramics in the polymer can produce dielectric capacitors with appropriate electric properties due to the high dielectric constant of the filler. However, activities on $BaTiO_3$ nanocomposites have not yielded a final product because of the problem of incompatibility as the matrix and reinforcing fillers have different surface characteristics, which makes a uniform dispersion of reinforcement fillers difficult to achieve and influences negatively the electrical properties of the final material [53]. The key factors which determine the properties of polymer nanocomposites include the percolation threshold, the nature of the nanofiller/matrix interface and the aspect ratio of the nanofiller [13]. Nanofillers can enhance both the function and structure of nanocomposites, for example, the addition of nanofiller with high intrinsic modulus can significantly improve the mechanical properties of polymer nanocomposites due to the strong bonding between the matrix and the nanofillers and uniform dispersion [13]. Percolation theory is used to study the change of dielectric properties in the nanocomposites system; the polymer nanocomposites can transition from insulator to conductor at a specific loading [13]. The percolation threshold is determined by the aspect ratio of the nanofillers [13]. Percolation is discussed in detail in Section 6.

The addition of rare-earth elements or functionalization has been reported to be a potential solution [24]. The dispersion of BTO nanoparticles can be improved by using surfactants, e.g. phosphate esters and oligomers v. Surfactants act as coupling agents with two different functional groups that attach to the matrix and surface of the filler separately creating a link [12]. Some works, such as Kim et al. [56] or Li et al. [57], have reported that the compatibility between $BaTiO_3$ and PVDF can be improved by using phosphoric acid and ethylene diamine although these two surfactants do not present strong binding with the BTO surface [12]. The selection of surfactants could be very important and the residual free surfactants can be the reason for high leakage current and dielectric loss which can also be influenced by the size of BTO nanoparticles [58]. Commonly, stirring has been applied for the dispersion to facilitate the interaction between BTO and the surfactants, which in some cases can be ineffective resulting in the reduction of compatibility [12]. To overcome the disadvantages of

stirring, Lin et al. [12] used the reflux method **(Figure 7)** in combination with dopamine, which is a green surface coupling agent. This technique has been widely used for nanoparticle surface modification since then [59]. Dopamine has been used for surface modification of BTO and it was found that an extended effective stirring time leads to an improvement in the chemical binding and dispersion of the nanoparticles within the polymer matrix as confirmed from SEM studies and other relevant characterization [59]. Overall, dopamine has been proved to be promising to enhance the nanoparticle-polymer interface and to promote a homogenous dispersion as well as a uniform charge at the interface of nanoparticle and polymer. **Figure 8** details the functionalization process [12,60]. Dopamine has been also been widely used for adhesion or surface coating such as MnO_2 for energy storage [61] and can be easily bio-synthesized [62]. Dopamine uses hydrogen bonding to bind strongly with different metals or metal oxides. A reaction between the NH_2 group of dopamine and C-F groups of PVDF can be expected which leads to a nanocomposite with improved compatibility. FESEM images (**Figure 9**) confirm that surface modification increases the homogeneity of particle dispersion [12]. Composites functionalized by dopamine have a dielectric constant of 26.8 and low dielectric loss of 0.04. **Figure 10** illustrates the dielectric properties of nanocomposites prepared using pristine and functionalized BTO. Lin et al. [12] have also synthesized hollow $BaTiO_3$ nanoparticles by the hydrothermal method without using a surfactant. **Figures 11-12** show FESEM and TEM images of the synthesized hollow nanoparticles. Neodymium oxide can improve the dielectric performance of the nanocomposite $BaTiO_3$-Nd_2O_3/PVDF (**Figure 13).** Wang et al. [63] combined the works of Lin et al. [12] by adding Nd oxide and using dopamine to improve the bonding in samples synthesized by the sol-hydrothermal method. After adding dopamine, the nanocomposites obtained a very high dielectric constant and the discharged energy density was increased up to 12.5 J/cm^3 [63].

5.2 Grafting and co-polymers

The current strategies to improve the performance of dielectric capacitors can be separated into two types: (i) use of ceramics as fillers to improve the properties, with some other elements potentially added to achieve a better result; (ii) use of surface surfactants to produce dielectric capacitors with improved functions. Some researchers have adopted an alternative approach to enhance the dielectric properties by enhancing the performance of the polymer matrix. In this direction, PVDF and its copolymers have shown a great potential to be used as a dielectric matrix to enhance dielectric properties. Electron beam irradiation has been used to activate the PVDF backbone (**Figure 14**). It is important to control the radiation dose during the irradiation process. PVDF has C-C, C-H, and C-F bonding; the C-H bond is much weaker than the C-F bond so it can be assumed to be the first bond to break [11]. However, if the irradiation dose is too high, the C-F bond can also be broken which might cause undesirable results [64]. **Figure 14** shows the detail of the whole process: when the C-H bond is broken, oxygen fills the space; however, if the dose is too strong, the C-F bond also breaks resulting in degradation of the performance. Graft copolymerization with HEMA

monomer can be carried after the activation of the polymer backbone. The resulting graft copolymer has enhanced dielectric properties (**Figure 15**) which are primarily attributed to the highly polar characteristics of the HEMA monomer [11]. Thakur et al. [11] have grafted styrene monomer (PS) on PVDF by electron beam radiation. The hydrophobic styrene monomer was grafted onto the PVDF matrix to maintain the advantages of PVDF, which exhibits excellent dielectric properties and is easy to process while improving the stability of capacitors. **Figure 16** shows the detailed mechanism of grafting of styrene onto PVDF. The dielectric constant of co-polymers increases to 90 at 100 Hz at room temperature, which is seven times higher than the PVDF precursor, accompanied by low dielectric loss of around 0.005 at 1 kHz. **Figures 17-18** illustrate the detailed dielectric properties analysis. Several points need to be highlighted which can influence the properties of final products. The first is the radiation dose, the grafting percentage increases with an increased radiation dose up to 17.5% when the dose is 1.6 MRad [11]. When the radiation dose increases, an increasing number of radicals is generated on the backbone of the polymer and as a consequence the grafting percentage increases [11]. The percentage of grafting decreases over 1.6 MRad, which can be explained by the fact that high energy transfer activates intramolecular scission of the grafted branches, i.e. the active sites remaining on the growing grafted chains may attack the grafted branches around them and cause chain scission and chain termination simultaneously. The consequence of this is that the length of the grafted branches decreases leading to a reduction of the overall weight fraction of grafted polymer [11]. The reaction temperature and time are still the main governing factors. An increase in temperature increases decomposition and produces more free radicals and diffusion of monomers which increases the graft percentage [11]. Over the optimum temperature, the large number of chain-transfer reactions and increased molecular motion results in a reduction of grafting [11]. Time affects the result in the same way as radiation dose; issues may be caused when the reaction time is beyond the optimum time leading to grafting percentage reduction. The type of solvent also can affect the result of irradiation [11]. Thakur et al. [11] used toluene as reaction medium and for the same irradiation, dose grafting increased by up to 28%. Increasing the amount of toluene has a negative effect as the continuous growth of grafting chains is inhibited by the reduction in monomer concentration. The variation of monomer concentration has the same influence as other factors; the grafting percentage is optimum for a specific monomer concentration.

In addition to the graft copolymerization technique, bioinspired surface modification in an aqueous medium can enhance the dielectric properties of PVDF. **Figure 19** shows the detailed mechanism of surface engineering of PVDF polymer powder. Dopamine has been used to surface engineer PVDF that has been irradiated before, followed by application of the reflux method to strengthen the dopamine -PVDF bonding [3]. Dopamine can build strong interfaces with different materials through hydrogen bonding. Further bonding improvement can be achieved by the reaction between the NH_2 groups in dopamine and the OH groups in pre-irradiated PVDF [3] or PVDF directly. Surface modification of PVDF results in significant enhancement of dielectric properties (**Figure 20-21**). The effect of temperature on dielectric properties of pristine

and surface modified PVDF has also been investigated. At the same frequency, the dielectric constant increases with increasing temperature due to the enhanced fractional mobility of the polymers and promotion of the orientation of dipoles [3]. The dielectric properties of a polymer are not only governed by the charge distribution but also the statistical thermal motion of the polar group of the polymers. During heating up, the thermal expansion and the decrease of intermolecular forces result in the relaxation process of mobile molecular chains, leading to an increase of dielectric constant [3].

Metal oxides are commonly used to improve the dielectric properties of capacitors due to their high permittivity [65]. The increase of the average field in the polymer matrix leads to an improvement in the effective dielectric constant, whilst only a small amount of energy is stored in the high permittivity phase [56-57]. As a consequence of the significant permittivity difference between the matrix and the filler, the electric field is inhomogeneous, which limits the improvement in electric properties that can be achieved [65]. Therefore, research has attempted to develop new techniques to overcome the problems of low dielectric constant and associated low energy storage of polymers [65]. One of the ways put forward is by adding a different polymer in the PVDF based capacitor to improve dielectric properties. This method is accompanied by some problems, e.g. PVDF homopolymers and copolymers like P(VDF-HFP) are suffering from large ferroelectric hysteresis loss which makes them not suitable for use as film capacitors [56]. Co-polymers like P(VDF-TRFE-CFE) and P(VDF-TrFE-CTFE) terpolymers and some other relaxor ferroelectric polymers have been developed to overcome this problem [56]. However, the narrow hysteresis and low melting temperature (120ºC) these polymers present make them unsuitable for use in high-temperature conditions [66].

Addonizioa et al. [67] found that the solvent used during the preparation can affect the pH value and further influence the properties of the final product. Fluoropolymers are chemically inert but relatively susceptible to high energy radiation, such as electron and ion beam, plasma treatment or X-rays [68–70], which can be used to facilitate attachment of functional groups onto the polymer surface. However, copolymers produced by grafting are limited in terms of quantity, as the production method cannot be scaled up due to the large copper catalyst consumption [68]. Furthermore, when PVDF is directly exposed to high positive voltage erosion and electrochemical reaction, issues may occur [71-72]. Yin et al.[68] used the force assembly technique to microlayer a linear dielectric polymer and PVDF based polymer to produce co-polymers to overcome these problems. Following modification, the α_c relaxation from the α PVDF crystals is reduced to a minimum in PET/PMMA/P(VDF-HFP) multilayer films and the loss from impurity ions is also minimized because of the use of PMMA with P(VDF-HFP) which modifies the interface between P(VDF-HFP) and PET layers [68].

Previous research on co-polymer produced by PVDF and TrFE indicates that the dielectric constant of some polymers increases after high energy electron irradiation treatment at room temperature if the dosage of the irradiation is appropriate [73]. Furthermore, after irradiation treatment, the polymer transforms from a normal ferroelectric into a relaxor ferroelectric. This eliminates the large polarization-field

hysteresis under the high field, especially in normal ferroelectric co-polymers [14]. PVDF exhibits much higher dielectric constant after modification in comparison with the pristine polymer and much lower dielectric loss [3]. Also, better flexibility was observed [3]. The excellent mechanical and electrical properties, as well as its biocompatibility, make PVDF a highly appropriate material for capacitors or power storage devices [74].

6. Effects of other factors:

6.1 pH value

Different synthesis of the raw materials has been studied since the preparation process can result in changes in the particle size and morphology which can directly affect the dielectric properties of the nanocomposites. Different preparation techniques such as sol-gel, hydrothermal and aqueous influence differently the properties of the final product as they introduce variations in different morphology, crystallinity and particle size [75–79]. Sol-gel synthesis has been widely applied due to its multifunctionality, easiness of processing and scalability. Oxides prepared by this technique are appropriate for coating or printing [80–82]. **Figure 22** illustrates generic sol-gel synthesis. Gilliot. et al. [26] showed that metal oxides prepared by sol-gel methods have an improved morphology and orientation which may lead to improved dynamic properties. Although the sol-gel technique can produce specimens with appropriate properties, control of this technique and details of the synthesis affecting the properties require further investigation. Addonizioa et al. [67] followed the work of Tari et al. [83] to investigate how the pH affects ZnO films produce by the sol-gel synthesis. In the work of Tari et al.[83], the stabilizer agents were Triethanolamine (TEA) and acetic acid, in addition to zinc acetate dihydrate (ZAD) alcoholic solutions with ZAD stabilizer agent (the molar ratio was equal to 1), with Zn^{2+} concentrations between 0.5-1.2 M [83]. Addonizio et al. [67] have also studied how the pH value influences the properties of films by controlling the minimum and maximum pH between 7.66 and 8.76 and comparing pure ZnO and B- or Al-doped ZnO to assess variations on thickness, morphology and optical properties [67]. The quality improvement of films by controlling the pH was also investigated in other works. Sagar et al. [84] controlled the pH range between 6.4 and 10.6 by using a different aliquot of monoethanolamine (MEA) in the initial 0.6M ZAD solution to produce the multi-layer films whose thickness was about 200nm. Improved quality of the multi-layer film was observed with the increase of pH, which is a result consistent with those obtained by Addonizio et al. Houng et al. [85] and Ilican et al. [86] using glacial acetic and ammonia to control the pH range between 5.0 to 6.8 and 5.05 to 7.15 respectively. This work demonstrated that electrical and optical properties can be improved by increasing the pH during the synthesis procedure [84]. The quality of films is not the only characteristic that the pH value can control, the minimum thickness that the films also depends on the concentration of the raw material solution and the type and amount of stabilizer agent [67]. Current

strategies for the improvement based on this concept include two approaches: (a) improve the preparation procedure; (b) addition of a dopant such as trivalent cations (B^{3+} or Al^{3+} for example) and hydrogen [67].

6.2 Annealing temperature

Besides the pH, the annealing temperature is considered as another main factor controlling the properties of the films during the synthesis process. Omri et al. [25] investigated how the thermal treatment can influence the electrical properties, structure, and morphology of ceramic (ZnO) nanoparticles. The objective of the investigation was to prepare high-quality crystalline ZnO nanoparticles at low temperature (300, 400 and 500ºC) [87]. The material treated at these temperatures showed variations in electrical properties at grain boundaries and grains, resulting in behavior corresponding to a material with regions of different conductivities [87]. Similar work was carried out by Kuo et al. [22], in which the variation of dielectric properties of epoxy/BaTiO3 nanocomposites with different ceramic content was tested under variable temperature and frequency. The nanocomposite with the highest content of ceramic filler treated at 900ºC has the highest dielectric constant; however, this value decreases with further increase in temperature [22]. As a consequence, the effect of temperature is very similar with the addition of dopant; an increase of dopant can enhance the dielectric properties of the nanocomposite; however, if the amount of dopant is too high the properties are degraded.

6.3 Synthesis techniques

The synthesis technique can affect significantly the microstructure of ceramics which influences the electrical performance. The sol-gel method has attracted much attention due to the relatively mild reaction conditions and the excellent particle distribution, high purity, homogeneity, and compositional control of powders obtained from this synthesis technique [87]. In contrast to the sol-gel process, the hydrothermal method can operate at low temperature and produce well-crystallized products [88-89]. The idea of investigating a new synthesis technique by combining these two methods was explored and a new method called sol-gel-hydrothermal has been reported [90–93] which can have the advantages of both techniques. More particularly, this new process is expected to be able to produce ceramics with high purity, narrow particle size distribution and high crystallinity, low process temperature and relatively controlled morphology.

Wang et al. [87] have used the sol-gel hydrothermal technique to prepare BaTiO3 nanoparticles using barium acetate and tetrabutyl titanate as the raw materials and acetic acid and absolute ethanol as the solvent. As a result of using KOH at a concentration of over 1.0 M calcined at 120ºC for 12h, the BaTiO3 is well-crystallized, with high purity and a uniform cubic structure [87]. Earlier work has shown that the temperature and reaction time could affect the microstructure of nanoparticles [75]; however, Lin et al. [64] have reported that the increase in the reaction time and temperature over a certain value can influence the crystallinity and morphology only slightly, while the concentration of KOH governs the variation of particle size and crystallinity [87]. The

particle size of $BaTiO_3$ decreases from 370 nm to 100 nm when the concentration of KOH increases from 1.0 M to 8.0 M [87].

Magnetron sputtering can be used to manufacture films by depositing target materials on hot glass substrates with radiofrequency or direct current under pressure [94]. Partial oxygen pressure during the process has a significant influence. Liu et al. [95] investigated the morphology, microstructure, surface, optical and electronic properties of ZnO and Cu doped ZnO films manufactured by magnetron co-sputtering with varying oxygen partial pressure. Reduction of crystallinity and bandgap was observed, which occurred due to the oxygen vacancy [96]. This phenomenon only occurred in films doped with Cu; ZnO films without doping did not show any sensitivity to oxygen pressure, especially at high pressures [95]. The substrate temperature can also be an influential factor; Ali et al. [96] have investigated the optical and dielectric behavior of ZnO films prepared with substrate temperature ranging from 100ºC to 500ºC. X-ray and AFM results showed that the deposition temperature influences the polycrystalline structure and crystallinity as well as the grain size [96]. Increasing the substrate temperature during deposition causes a reduction of the optical energy gap attributed to the increase of the degree of crystallinity and the number of free electrons [96]. The thickness of the film is also an influencing factor. Pathak et al. [97] investigated the structural and optical properties and morphology of ZnO films prepared by sol-gel synthesis. The surface morphological studies indicated that an increase in the film thickness can lead to a grain size increase as well as an increase in film roughness and reduction of the bandgap [97]. The same conclusion can also be applied to films synthesized by glass substrates spraying [98].

Depending on the synthesis conditions, the nanoparticles can have different morphology, even if the same preparation technique is applied. Mao et al. [99] have successfully synthesized one-dimensional BaTiO3 and $SrTiO_3$ nanotubes by using the hydrothermal technique at low temperature, aiming to overcome issues with the conventional method for the preparation of BTO structure nanoparticles associated with the high pressure, temperature and surface functionalization process. The one-dimensional character of nanotube or nanowire systems is ideal for investigating the effect of size and dimensions on optical, magnetic and electronic properties [99]. According to previous work, the structure and reactivity of barium, strontium, and titanium precursors are the key factors that determine the composition, particle size, morphology and properties of the final nanoparticles [64]. The hydrothermal method has been applied for the preparation of ceramic power especially barium titanium for decades; the strategy of Mao et al. was based on the use of TiO_2 nanotube as a precursor. Lin et al. [64] used the same synthesis technique to synthesize single-crystalline Nd-doped BaTiO3 hollow nanoparticles at low temperature without the use of a surfactant or high-temperature sintering. Lin et al. [64] also used Nd oxides as dopant added into the BaTiO3 to obtain a high dielectric constant taking into account the high dielectric constant (K=300000) that Nd oxide has after high temperature firing under pure nitrogen. Besides, the ionic radius of neodymium is between those of titanium and barium which means that neodymium can fit in barium or titanium sites leading to an improved permittivity [64]. The hollow nanostructure that Lin et al. [64] synthesized

has a poor dielectric constant due to the presence of air voids in the structure. Lin et al. [64] have successfully overcome the shortcomings of the nano hollow structure, as the dielectric constant of the final products is nearly 5 times higher than the value from previous works (40.7 at 103 Hz). The synthesis temperature is a very important factor for the successful synthesis as also found by Omri et al. [25]. The morphologies of the nanoparticles vary from spherical solid particle to hollow structure with increasing temperature, which indicates that the temperature can influence the diffusion rate of Nd ions into the BTO structure and directly determine the morphology of the final product [64]. The reaction time can also be an influencing factor; an increase of reaction time increases the particle size [64] while a reduction of grain size is associated with a reduction of the dielectric constant [22]. Therefore, the balance between temperature and reaction time needs to be carefully controlled. The formation of hollow nanostructures is governed by the Kirkendall mechanism [64]. This governs the diffusion of metal atoms when the temperature is high enough to activate the diffusion of atoms from metal A to metal B or the opposite [100]. Modelling studies have also been carried out to understand the dielectric properties of graphite-polymer composites [65]. Xia et al [65] have developed a thermodynamic framework to explain dielectric damage concerning the applied electric field. The developed theory was validated using experimental data from PVDF-Graphite composites. The breakdown strength of the nanocomposite decreases with the amount of graphite which is also reflected in an increment in the energy storage density. **Figure 23** summarizes the dielectric behavior of graphene polymer nanocomposites.

Among the different microstructure morphology, 1-D fillers such as nanowires and nanofibers are proved to enhance the dielectric properties of nanocomposites more efficient [101]. Huang et al. [101] conclude the advantages of using high aspect ratio 1D fillers to produce nanocomposites with high dielectric constant are: (i) high aspect ratio fillers can reach contact percolation easier than lower aspect ratio fillers which allow the fillers to be continuously transported into the composites and enhance the dielectric properties or higher thermal conductivity; (ii) high aspect ratio fillers have a lower surface area which can help to reduce the surface energy and prevent aggregation especially when the filler content is high; (iii) high aspect ratio fillers can enhance the composites with lower loading due to their large dipole moment. Among all the structures, core-shell structures have a high dielectric constant core but the dielectric constant of the shells is at middle level, while the dielectric constant tends to decrease from the core to the matrix [101]. The shell of the core-shell structured particles is usually the buffer between the core and the matrix of the composites that can reduce the electric field distortion and strengthen the dielectric properties of the polymer composites [101]. Furthermore, a small electric field enhancement was reported inside the core-shell particles, which is a depolarization field formed by the electric charges aggregated at the interface layer of the filler and matrix that eliminates part of the applied electric field inside the filler [101]. Yao et al. [102] compared the dielectric constant and breakdown strength of PVDF-HFP copolymer filled by $BaTiO_3$ and TiO_2 encapsulated $BaTiO_3$ nanoparticles. The material containing core-shell structured $BaTiO_3$ @TiO_2 exhibits an unexpectedly high dielectric constant nearly three times

higher than the material with $BaTiO_3$ at same filler volume fraction and a significantly improved breakdown strength. The preparation of core-shell structures is also carried out in different ways; recently, Bi et al.[103] synthesized core-shell BTO@SiO_2 by the Stober method. The influence study of the core shell structured $BaTiO_3$ @TiO_2 nanofillers on the energy storage ability on the nanocomposites confirm the advantage of this type of structure.

An alternative way to enhance the dielectric performance of nanocomposites is the use of inorganic conductive materials as fillers, such as carbon which has been investigated as a novel interfacial modifier [104]. Use of conventional inorganic materials, such as TiO_2 nanowires, as core and a conductive carbon layer as the shell, synthesized by hydrothermal reaction and chemical vapor deposition has been attempted [104]. An enhanced dielectric permittivity was observed which was nearly 80 times higher than that of the nanocomposites using untreated TiO_2 nanowires as filler, while by controlling the time of chemical vapor deposition process, the thickness of the interface can be modulated [104]. Another method to further strengthen the advantages of core-shell structure is to use multiple shells to provide a hierarchical functional interface layer; the outer layer can help the interaction and dispersion of the ceramic fillers in the nanocomposites, the inner polarization layer can promote the relative permittivity of the nanocomposites, while the buffer and shielding layers can eliminate the local electric field and decrease the electric loss by preventing the free electrons [104]. These strategies are only true for 0-3 type nanocomposites (0-3 type nanocomposites mean the composites formed by nanoparticles distributed in three-dimensional bulk materials), where the maximum loading could be around 50-60%.

Recently, topological structures including a sandwich or multi-layer structures have been reported to form 2-2 type composite, which means two-dimensional connected fillers dispersed in a two-dimensional connected polymer matrix and an extra insulating layer [104]. PVDF and PVDF co-polymer have been selected as the insulating layer because of their high dielectric strength and low dielectric loss [104]. For example, the use of P(VDF-HFP) as the central layer and BaTiO3/P(VDF-HFP) as upper and lower layers formed by spin-coating, can be used to produce a sandwich structure nanocomposite. The problem of this type of structure is the low relative permittivity and polarization due to the low relative permittivity of the central layer (polymer), whilst the solution is the addition of dopant, generally as a small amount of ceramic nanofiller such as $BaTiO_3$ nanofibers or boron nitride nanosheets and some other common ceramic nanofillers [104].

6.4 Volume fraction

Kim et al. [7] reported how the nanoparticle volume fraction influences the dielectric properties including the effective permittivity, dielectric loss and dielectric breakdown strength of phosphonic acid-modified BTO doped P(VDF-HFP) based co-polymer.

The experimental permittivity increases to a maximum when the volume fraction is around 50-60%, then decreases rapidly with the further increase of the nanoparticle volume fraction. The experimental values were compared with several models. (**Figure**

24) The large difference between experimental and models occur when the volume fraction above 60% [7]. Weibull statistics were used to compare the dielectric breakdown strength of the nanocomposites with BTO volume fractions between 0 and 50%. The Weibull analysis is based on the following expression for the failure probability [7]:

$$P_F(E) = 1 - \exp[-\left(\frac{E-\gamma}{\alpha}\right)^{\beta}] \quad (10)$$

Where β and γ is the shape parameter that shows the dispersion of E and the threshold parameter which value the E with no failure; α is the scale parameter. Kim et al assumed γ is zero so that the failure probability can be calculated by the following equation [7]:

$$\log[-\ln\{1 - P_F(E)\}] = \beta log E - \beta log \alpha \quad (11)$$

The dielectric breakdown strength with volume fraction higher than 50% is much lower than that of low volume fraction which can be explained by the existence of air voids in the nanocomposites [7]. Besides, the breakdown strengths of the nanocomposites over 50% of void fraction changes significantly between each sample due to the variation of porosity distribution which also explained why the calculation is valid for low volume fraction [7]. **Figure 25** illustrates the breakdown strength obtained by Weibull analysis at different volume fraction with 63.2% failure probabilities. The dielectric strength decreases rapidly when the volume fraction increases from 10%~20%, such behavior can be explained by the percolation of the BTO nanoparticles in the composite. Calame [105] described the percolation in detail; percolation in the composites needs to be considered in two different ways: "hard" and "soft" percolation. Soft percolation means connected particles tend to generate an extended network which provides a pathway [7]. As a result, the charge conduction can cause breakdown strength reduction; furthermore, such behavior can lead to ineffective surface modification, due to passivation and reduction of ionizable surface sites because of the phosphonate layer [7]. Hard percolation can occur with the further increase of volume fraction and maximum particle density achieved [7]. When most of the particles are in contact with each other and the particle density cannot be changed further increase of particles leads to v increase of air voids as the polymer is not enough to fill the interstitial free volume [7]. The dielectric breakdown strength depends on the distribution of air voids since the nanoparticles entering the polymer are packed randomly; the air voids are also distributed randomly which justifies the large difference between experimental data and the model.[7]. Another noticeable point is that the failure probability of P(VDF-FHP) film is higher than that of the nanocomposites with 5% and 10% BTO (**Figure 25 a**). This implies that the addition of filler with high permittivity into the polymer under conditions of "soft" percolation can control the failure probability under moderate fields, while the nanoparticles can trap the charges and prevent them to scatter in the nanocomposite film to increase the failure probability [7].

The volume fraction of air voids can be computed by the cellular packing model [105]. Kim et al. [7] use this model to predict the maximum volume fraction that can be obtained without creating any air voids (**Figure 26**). This model cannot simulate the

maximum density situation [7]. The volume fraction of air voids can be estimated by the expression:

$$V(F) = a(f - f_T)^p \quad (12)$$

where f is the volume fraction, f_T is the threshold volume fraction when there are no voids in the composite and), a and p are fitting parameters [7]. **Figure 27** shows the experimental and calculated breakdown strength at different volume fractions; the difference is because the films were fabricated by a spin coating which is a kinetically controlled process which allows the reduction of the concentration of air voids and improvement of film quality [7].

Eq. 2 suggests that maximum volume fraction can be used to achieve the maximum energy density. **Figure 28** shows the calculated and experimented energy density with different nanoparticle volume fraction at fixed applied electric field (164 V/μm) and 1 MHz. The two data groups show a similar trend but the measured values are lower than the calculated values, partially because the energy density measurement depends on the breakdown strength, which means the energy density cannot be tested at high volume fraction [7].

All the nanocomposites, their modification and the influence factors mentioned in the context before are summarized in **Table S1**.

7. Conclusion

In addition to the modification and synthesis techniques described in this article, many other strategies can also be applied to improve the performance of capacitors[106]. Research on capacitors will be addressing problems over the long term. For example, the energy density of a polymer-based nanocomposite is determined by the dielectric constant and breakdown strength. All the modifications mentioned in this article are used to improve the bonding between matrix and filler so that the capacitors can have a better breakdown strength. Therefore, the study on polarization is still ongoing focusing on polarization mechanisms customization. The full understanding of the working mechanisms will contribute to the design of capacitors exhibiting satisfactory performance. However, developing a complete understanding and control is not a short-term objective. In theory, it is easier to improve electronic polarization by delocalizing electrons, but during the process, material selection could be a problem. Therefore, the complete understanding of dielectric performance requires not only the understanding of how to produce high-performance capacitors but also the need to select appropriate materials. Some materials or ceramic fillers have great properties but contain lead which is harmful to the environment, while non-lead ceramics cannot reach a satisfactory result yet. Another example is ionic polarization; replacing the carbon in the polymer by other elements such as group 14 elements can tailor the ionic polarization. However, the synthesis of such polymer is full of challenges. Problems associated with the modification also need to be resolved. One of the modification methods described in this article is the addition of dopant in nanocomposites. Under most of the conditions, the dielectric constant increases with increasing doping up to a maximum value beyond which the performance decreases. Using the maximal value of doping can achieve the desired dielectric performance. However, there is also a limit of

doping concerning higher dielectric loss due to incompatibility and agglomeration issues. Aggregation can cause further problems such as the concentration of the electric field in the matrix which leads to lower breakdown strength; even lower than that of the pure polymer. Many works have used a surface modification to overcome this situation. The application of surface modification is based on the fact that appropriate surfactants can improve the bonding between matrix and filler by covalent bonding, hydrogen bonding or dipole-dipole interactions; homogeneous nanocomposites can be obtained as a result of the improved interaction. While the problem is choosing the right surface-modifying agents, depending on the material used, the performance of capacitors after modification can be very different even for the same surfactant. Other approaches, such as grafting, are limited in production due to scalability issues.

As a conclusion, a large number of modification techniques related to the improvement of dielectric properties of polymer-based nanocomposites have been summarized in this article. However, there are still many problems that are worth investigating and need to be overcome[106]. An ideal capacitor matrix material needs to have high energy and power density, suitable functional groups, low dielectric loss, great compatibility with reinforcing materials and being easy to manufacture.

8. References:

[1] M. Y. Ho, P. S. Khiew, D. Isa, T. K. Tan, W. S. Chiu, and C. H. Chia, "A review of metal oxide composite electrode materials for electrochemical capacitors," *Nano*, vol. 9, no. 6, pp. 1–25, 2014, doi: 10.1142/S1793292014300023.

[2] L. Yang *et al.*, "Perovskite lead-free dielectrics for energy storage applications," *Prog. Mater. Sci.*, vol. 102, no. May 2018, pp. 72–108, 2019, doi: 10.1016/j.pmatsci.2018.12.005.

[3] V. K. Thakur, M. F. Lin, E. J. Tan, and P. S. Lee, "Green aqueous modification of fluoropolymers for energy storage applications," *J. Mater. Chem.*, vol. 22, no. 13, pp. 5951–5959, 2012, doi: 10.1039/c2jm15665b.

[4] V. Kumar, A. Kumar, R. R. Wu, and D. J. Lee, "Room-temperature vulcanized silicone rubber/barium titanate–based high-performance nanocomposite for energy harvesting," *Mater. Today Chem.*, vol. 16, 2020, doi: 10.1016/j.mtchem.2019.100232.

[5] Q. Li, F.-Z. Yao, Y. Liu, G. Zhang, H. Wang, and Q. Wang, "High-Temperature Dielectric Materials for Electrical Energy Storage," *Annu. Rev. Mater. Res.*, vol. 48, no. 1, pp. 219–243, 2018, doi: 10.1146/annurev-matsci-070317-124435.

[6] Prateek, V. K. Thakur, and R. K. Gupta, "Recent Progress on Ferroelectric Polymer-Based Nanocomposites for High Energy Density Capacitors: Synthesis, Dielectric Properties, and Future Aspects," *Chem. Rev.*, vol. 116, no. 7, pp. 4260–4317, 2016, doi: 10.1021/acs.chemrev.5b00495.

[7] P. Kim *et al.*, "High energy density nanocomposites based on surface-modified BaTiO3 and ferroelectric polymer," *ACS. Nano.*, vol. 3, no. 9, pp. 2581–2592,

2009, doi: 10.1021/nn9006412.
[8] X. Dou, X. Liu, Y. Zhang, H. Feng, J. F. Chen, and S. Du, “Improved dielectric strength of barium titanate-polyvinylidene fluoride nanocomposite,” *Appl. Phys. Lett.*, vol. 95, no. 13, 2009, doi: 10.1063/1.3242004.
[9] Z. M. Dang, H. Y. Wang, and H. P. Xu, “Influence of silane coupling agent on morphology and dielectric property in BaTiO3/polyvinylidene fluoride composites,” *Appl. Phys. Lett.*, vol. 89, no. 11, pp. 87–90, 2006, doi: 10.1063/1.2338529.
[10] V. K. Thakur, E. J. Tan, M. F. Lin, and P. S. Lee, “Poly(vinylidene fluoride)-graft-poly(2-hydroxyethyl methacrylate): A novel material for high energy density capacitors,” *J. Mater. Chem.*, vol. 21, no. 11, pp. 3751–3759, 2011, doi: 10.1039/c0jm02408b.
[11] V. K. Thakur, E. J. Tan, M. F. Lin, and P. S. Lee, “Polystyrene grafted polyvinylidenefluoride copolymers with high capacitive performance,” *Polym. Chem.*, vol. 2, no. 9, pp. 2000–2009, 2011, doi: 10.1039/c1py00225b.
[12] M. F. Lin, V. K. Thakur, E. J. Tan, and P. S. Lee, “Surface functionalization of BaTiO3 nanoparticles and improved electrical properties of BaTiO3/polyvinylidene fluoride composite,” *RSC Adv.*, vol. 1, no. 4, pp. 576–578, 2011, doi: 10.1039/c1ra00210d.
[13] C. Yang *et al.*, “Polymer nanocomposites for energy storage, energy saving, and anticorrosion,” *J. Mater. Chem. A*, vol. 3, no. 29, pp. 14929–14941, 2015, doi: 10.1039/c5ta02707a.
[14] Q. M. Zhang, V. Bharti, and X. Zhao, “Giant electrostriction and relaxor ferroelectric behavior in electron- irradiated poly(vinylidene fluoride-trifluoroethylene) copolymer,” *Science.*, vol. 280, no. 5372, pp. 2101–2104, 1998, doi: 10.1126/science.280.5372.2101.
[15] S. Das, and A. Ghosh, “Symmetric electric double-layer capacitor containing imidazolium ionic liquid-based solid polymer electrolyte: Effect of TiO2 and ZnO nanoparticles on electrochemical behavior,” *J. Appl. Polym. Sci.*, vol. 137, no. 22, pp. 23–25, 2020, doi: 10.1002/app.48757.
[16] M. Guo, J. Jiang, Z. Shen, Y. Lin, C. W. Nan, and Y. Shen, “High-Energy-Density Ferroelectric Polymer Nanocomposites for Capacitive Energy Storage: Enhanced Breakdown Strength and Improved Discharge Efficiency,” *Mater. Today*, vol. 29, pp. 49–67, 2019, doi: 10.1016/j.mattod.2019.04.015.
[17] E. R. Ezeigwe, M. T. T. Tan, P. S. Khiew, and C. W. Siong, “One-step green synthesis of graphene/ZnO nanocomposites for electrochemical capacitors,” *Ceram. Int.*, vol. 41, no. 1, pp. 715–724, 2015, doi: 10.1016/j.ceramint.2014.08.128.
[18] Z. S. Wu, G. Zhou, L. C. Yin, W. Ren, F. Li, and H. M. Cheng, “Graphene/metal oxide composite electrode materials for energy storage,” *Nano Energy*, vol. 1, no. 1, pp. 107–131, 2012, doi: 10.1016/j.nanoen.2011.11.001.
[19] H. J. Choi, S. M. Jung, J. M. Seo, D. W. Chang, L. Dai, and J. B. Baek, “Graphene for energy conversion and storage in fuel cells and

supercapacitors," *Nano Energy*, vol. 1, no. 4, pp. 534–551, 2012, doi: 10.1016/j.nanoen.2012.05.001.

[20] B. Saravanakumar, R. Mohan, and S. J. Kim, "Facile synthesis of graphene/ZnO nanocomposites by low temperature hydrothermal method," *Mater. Res. Bull.*, vol. 48, no. 2, pp. 878–883, 2013, doi: 10.1016/j.materresbull.2012.11.048.

[21] W. Han *et al.*, "Self-assembled three-dimensional graphene-based aerogel with embedded multifarious functional nanoparticles and its excellent photoelectrochemical activities," *ACS Sustain. Chem. Eng.*, vol. 2, no. 4, pp. 741–748, 2014, doi: 10.1021/sc400417u.

[22] D. H. Kuo, C. C. Chang, T. Y. Su, W. K. Wang, and B. Y. Lin, "Dielectric behaviours of multi-doped BaTiO3/epoxy composites," *J. Eur. Ceram. Soc.*, vol. 21, no. 9, pp. 1171–1177, 2001, doi: 10.1016/S0955-2219(00)00327-7.

[23] C. W. Reed and S. W. Cichanowski, "The Fundamentals of Aging in HV Polymer-film Capacitors," *IEEE Trans. Dielectr. Electr. Insul.*, vol. 1, no. 5, pp. 904–922, 1994, doi: 10.1109/94.326658.

[24] B. J. Chu *et al*., "A Dielectric Polymer with high electric energy density and fast discharge speed," *Science*., vol. 313, no. 5785, pp. 334–336, 2006, doi: 10.1126/science.1127798.

[25] K. Omri, I. Najeh, and L. El Mir, "Influence of annealing temperature on the microstructure and dielectric properties of ZnO nanoparticles," *Ceram. Int.*, vol. 42, no. 7, pp. 8940–8948, 2016, doi: 10.1016/j.ceramint.2016.02.151.

[26] M. Gilliot, A. Hadjadj and A.E. Naciri, "Dielectric function of very thin nano-granular ZnO layers with different states of growth," Appl. Opt., vol. 54, no. 10, pp. 3043-3050, 2015, doi:org/10.1364/AO.54.003043.

[27] T. Brousse and D. Bélanger, "A Hybrid FeO-MnO Capacitor in Mild Aqueous Electrolyte," *Electrochem. Solid-State Lett.*, vol. 6, no. 11, p. A244, 2003, doi: 10.1149/1.1614451.

[28] P. Simon and Y. Gogotsi, "Materials for electrochemical capacitors," *Mater. Sustain. Energy A Collect. Peer-Reviewed Res. Rev. Artic. from Nat. Publ. Gr.*, pp. 138–147, 2010, doi: 10.1142/9789814317665_0021.

[29] G. H. Yuan, Z. H. Jiang, A. Aramata, and Y. Z. Gao, "Electrochemical behavior of activated-carbon capacitor material loaded with nickel oxide," *Carbon N. Y.*, vol. 43, no. 14, pp. 2913–2917, 2005, doi: 10.1016/j.carbon.2005.06.027.

[30] Y. Wang, H. Liu, X. Sun, and I. Zhitomirsky, "Manganese dioxide-carbon nanotube nanocomposites for electrodes of electrochemical supercapacitors," *Scr. Mater.*, vol. 61, no. 11, pp. 1079–1082, 2009, doi: 10.1016/j.scriptamat.2009.08.040.

[31] X. Liu *et al.*, "One-step electrochemical deposition of nickel sulfide/graphene and its use for supercapacitors," *Ceram. Int.*, vol. 40, no. 6, pp. 8189–8193, 2014, doi: 10.1016/j.ceramint.2014.01.015.

[32] Z. Fan and J. G. Lu, "Zinc oxide nanostructures: Synthesis and properties," *J. Nanosci. Nanotechnol.*, vol. 5, no. 10, pp. 1561–1573, 2005, doi:

10.1166/jnn.2005.182.
[33] Y. Zhu *et al.*, “Multiwalled carbon nanotubes beaded with ZnO nanoparticles for ultrafast nonlinear optical switching,” *Adv. Mater.*, vol. 18, no. 5, pp. 587–592, 2006, doi: 10.1002/adma.200501918.
[34] F. T. Johra, M. J. Lee, and W. G. Jung, “Solution-based fabrication of a graphene-ZnO nanocomposite,” *J. Sol-Gel Sci. Technol.*, vol. 66, no. 3, pp. 481–487, 2013, doi: 10.1007/s10971-013-3035-4.
[35] K. Kinoshita and A. Yamaji, “Grain-size effects on dielectric properties in barium titanate ceramics,” *J. Appl. Phys.*, vol. 47, no. 1, pp. 371–373, 1976, doi: 10.1063/1.322330.
[36] W. R. Buessem, L. E. Cross and A. K. Goswami, “Phenomenological Theory of High Permittivity in Fine Grained Barium Titanate,” A.C. Society., vol. 49, no. 1, 1966, doi: 10.1111/j.1151-2916.1966.tb13144.x.
[37] S. Zemouli, A. Chaabi, and H. S. Talbi, “Design of a compact and high sensitivity temperature sensor using metamaterial,” *Int. J. Antennas Propag.*, vol. 2015, 2015, doi: 10.1155/2015/301358.
[38] H. J. Hwang, T. Nagai, T. Ohji, M. Sando, M. Toriyama, and K. Niihara, “Curie Temperature Anomaly in Lead Zirconate Titanate/Silver Composites,” *J. Am. Ceram. Soc.*, vol. 81, no. 3, pp. 709–712, 2005, doi: 10.1111/j.1151-2916.1998.tb02394.x.
[39] T. Hiroshima, K. Tanaka, and T. Kimura, “Effects of microstructure and composition on the curie temperature of lead barium niobate solid solutions,” *J. Am. Ceram. Soc.*, vol. 79, no. 12, pp. 3235–3242, 1996, doi: 10.1111/j.1151-2916.1996.tb08100.x.
[40] H. Kanai,O. Furukawa, S. Nakamura and Y, Yamashita, “Effect of Stoichiometry on the Dielectric Properties and Life Performance of $(Pb_{0.875}Ba_{0.125})$ $[(Mg_{1/3}Nb_{2/3})_{0.5}$ $Zn_{1/3}Nb_{2/3})_{0.3}$ $Ti_{0.2}]O_3$ Relaxor Dielectric Ceramic: Part I, Dielectri. Properties, ” *J. Am. Ceram. Soc.*, vol. 76, no. 2, pp. 454-458, 1993, doi: 10.1111/j.1151-2916.1993.tb03806.x.
[41] S. Ducharme, “An inside-out approach to storing electrostatic energy,” *ACS Nano*, vol. 3, no. 9, pp. 2447–2450, 2009, doi: 10.1021/nn901078s.
[42] E. H. Kerner, “The electrical conductivity of composite media,” *Proc. Phys. Soc. Sect. B*, vol. 69, no. 8, pp. 802–807, 1956, doi: 10.1088/0370-1301/69/8/304.
[43] D. E. Aspnes, “Local field effects and effective medium theory: A microscopic perspective,” Am. J. Phys., vol. 704, no. 50, pp. 28–31, 1998, doi: 10.1119/1.127342.
[44] N. Jayasundere and B. V. Smith, “Dielectric constant for binary piezoelectric 0-3 composites,” *J. Appl. Phys*., vol. 73, no. 5, 1998, doi: 10.1063/1.354057.
[45] Z. Du, B. Ozpineci, L. M. Tolbert, and J. N. Chiasson, “DC-AC cascaded H-bridge multilevel boost inverter with no inductors for electric/hybrid electric vehicle applications,” *IEEE Trans. Ind. Appl.*, vol. 45, no. 3, pp. 963–970, 2009, doi: 10.1109/TIA.2009.2018978.
[46] M. S. Whittingham, “Materials challenges facing electrical energy storage,”

MRS Bull., vol. 33, no. 4, pp. 411–419, 2008, doi: 10.1557/mrs2008.82.
[47] Y. Yang *et al.*, "Three dimensional printing of high dielectric capacitor using projection based stereolithography method," *Nano Energy*, vol. 22, pp. 414–421, 2016, doi: 10.1016/j.nanoen.2016.02.045.
[48] K. Kim *et al.*, "3D optical printing of piezoelectric nanoparticle-polymer composite materials," *ACS Nano*, vol. 8, no. 10, pp. 9799–9806, 2014, doi: 10.1021/nn503268f.
[49] D. Gonzalez, L. Noble, B. Newell, T. Mamer, and J. Garcia, "3-D printing of dielectric electroactive polymer actuators and characterization of dielectric flexible materials," *ASME 2018 Conf. Smart Mater. Adapt. Struct. Intell. Syst. SMASIS 2018*, vol. 2, pp. 1–6, 2018, doi: 10.1115/SMASIS2018-8011.
[50] D. Williams, "Physical principles of defibrillators," *Anaesth. Intensive Care Med.*, vol. 13, no. 8, pp. 384–387, 2012, doi: 10.1016/j.mpaic.2012.05.011.
[51] Y. Shen, X. Zhang, M. Li, Y. H. Lin and C. W. Nan, "Polymer nanocomposite dielectric for electrical energy storage," Natl. Sci. Rev., vol. 4, no. 1, pp. 23-25, 2017, doi: 10.1093/nsr/nww066.
[52] Y. Shen, Y. Lin, and Q. M. Zhang, "Polymer nanocomposites with high energy storage densities," *MRS Bull.*, vol. 40, no. 9, pp. 753–759, 2015, doi: 10.1557/mrs.2015.199.
[53] C. Huang and Q. Zhang, "Enhanced dielectric and electromechanical responses in high dielectric constant all-polymer percolative composites," *Adv. Funct. Mater.*, vol. 14, no. 5, pp. 501–506, 2004, doi: 10.1002/adfm.200305021.
[54] Y. Rao and C. P. Wong, "Material Characterization of a High-Dielectric-Constant Polymer-Ceramic Composite for Embedded Capacitor for RF Applications," *J. Appl. Polym. Sci.*, vol. 92, no. 4, pp. 2228–2231, 2004, doi: 10.1002/app.13690.
[55] K. R. Mikeska and W. R. Cannon, "Non-aqueous dispersion properties of pure barium titanate for tape casting," *Colloids and Surfaces*, vol. 29, no. 3, pp. 305–321, 1988, doi: 10.1016/0166-6622(88)80125-2.
[56] P. Kim *et al.*, "Phosphonic acid-modified barium titanate polymer nanocomposites with high permittivity and dielectric strength," *Adv. Mater.*, vol. 19, no. 7, pp. 1001–1005, 2007, doi: 10.1002/adma.200602422.
[57] J. Li, J. Claude, L. E. Norena-Franco, S. Il Seok, and Q. Wang, "Electrical energy storage in ferroelectric polymer nanocomposites containing surface-functionalized BaTiO3 nanoparticles," *Chem. Mater.*, vol. 20, no. 20, pp. 6304–6306, 2008, doi: 10.1021/cm8021648.
[58] Z. M. Dang, H. Y. Wang, B. Peng, and C. W. Nan, "Effect of BaTiO3 size on dielectric property of BaTiO 3/PVDF composites," *J. Electroceramics*, vol. 21, no. 1-4 SPEC. ISS., pp. 381–384, 2008, doi: 10.1007/s10832-007-9201-8.
[59] R. Y. Hong *et al.*, "Synthesis, surface modification and photocatalytic property of ZnO nanoparticles," *Powder Technol.*, vol. 189, no. 3, pp. 426–432, 2009, doi: 10.1016/j.powtec.2008.07.004.
[60] Y. Song, Y. Shen, H. Liu, Y. Lin, M. Li, and C. W. Nan, "Enhanced dielectric and ferroelectric properties induced by dopamine-modified BaTiO 3 nanofibers

in flexible poly(vinylidene fluoride-trifluoroethylene) nanocomposites," *J. Mater. Chem.*, vol. 22, no. 16, pp. 8063–8068, 2012, doi: 10.1039/c2jm30297g.

[61] H. Jiang, L. Yang, C. Li, C. Yan, P. S. Lee, and J. Ma, "High-rate electrochemical capacitors from highly graphitic carbon-tipped manganese oxide/mesoporous carbon/manganese oxide hybrid nanowires," *Energy Environ. Sci.*, vol. 4, no. 5, pp. 1813–1819, 2011, doi: 10.1039/c1ee01032h.

[62] H. Lee, S. M. Dellatore, W. M. Miller, and P. B. Messersmith, "Mussel-Inspired Surface Chemistry for Multifunctional Coatings," Sci., vol. 318, no. 5849, pp. 426-430, 2007, doi: 10.1126/science.1147241.

[63] J. Wang *et al.*, "High discharged energy density of polymer nanocomposites induced by Nd-doped BaTiO3 nanoparticles," *J. Mater.*, vol. 4, no. 1, pp. 44–50, 2018, doi: 10.1016/j.jmat.2018.01.001.

[64] M. F. Lin, V. K. Thakur, E. J. Tan, and P. S. Lee, "Dopant induced hollow BaTiO3 nanostructures for application in high performance capacitors," *J. Mater. Chem.*, vol. 21, no. 41, pp. 16500–16504, 2011, doi: 10.1039/c1jm12429c.

[65] X. Xia, B. X. Xu, X. Xiao, and G. J. Weng, "Modeling the dielectric breakdown strength and energy storage density of graphite-polymer composites with dielectric damage process," *Mater. Des.*, vol. 189, p. 108531, 2020, doi: 10.1016/j.matdes.2020.108531.

[66] L. Zhu and Q. Wang, "Novel ferroelectric polymers for high energy density and low loss dielectrics," *Macromolecules*, vol. 45, no. 7, pp. 2937–2954, 2012, doi: 10.1021/ma2024057.

[67] M. L. Addonizio, A. Aronne, S. Daliento, O. Tari, E. Fanelli, and P. Pernice, "Sol-gel synthesis of ZnO transparent conductive films: The role of pH," *Appl. Surf. Sci.*, vol. 305, pp. 194–202, 2014, doi: 10.1016/j.apsusc.2014.03.037.

[68] K. Yin, Z. Zhou, D. E. Schuele, M. Wolak, L. Zhu, and E. Baer, "Effects of Interphase Modification and Biaxial Orientation on Dielectric Properties of Poly(ethylene terephthalate)/Poly(vinylidene fluoride-co-hexafluoropropylene) Multilayer Films," *ACS Appl. Mater. Interfaces*, vol. 8, no. 21, pp. 13555–13566, 2016, doi: 10.1021/acsami.6b01287.

[69] N. Walsby, F. Sundholm, and T. Kallio, "Radiation-Grafted Ion-Exchange. Membranes : Influence of the Initial Matrix on the Synthesis and Structure," *J. Poly.Sci.*, vol. 39, no. 17, pp. 3008–3017, 2001, doi: 10.1002/pola.1281

[70] H. P. Brack, H. G. Buhrer, L. Bonorand and G. G. Scherer, "Grafting of pre-irradiated poly(ethylene-alt-tetrafluoroethylene) films with styrene: influence of base polymer film properteis and processing parameters" *J. Mater. Chem.*, vol. 10, no. 8, pp. 1795-1803, 2000, doi:10.1039/B001851L.

[71] S. Hietala, S. L. Maunu, and F. Sundholm, "Structure of Styrene Grafted Poly(vinylidene fluoride) Membranes Investigated by Solid-State NMR," *Macromolecules*, vol. 32, no. 3, pp. 788–791, 1999, doi: 10.1021/ma981543k.

[72] G. Eberle, H. Schmidt, and W. Eisenmenger, "Influence of poling conditions on the gas emission of PVDF," *Annu. Rep. - Conf. Electr. Insul. Dielectr. Phenom.*, pp. 263–268, 1993, doi: 10.1109/ceidp.1993.378962.

[73] M. Ponting, A. Hiltner, and E. Baer, “Polymer nanostructures by forced assembly: Process, structure, and properties,” *Macromol. Symp.*, vol. 294, no. 1, pp. 19–32, 2010, doi: 10.1002/masy.201050803.

[74] Y. Bai, V. Bharti, H. S. Xu, Q. M. Zhang, and V. Affiliations, “High-dielectric-constant ceramic-powder polymer composites,” *Appl. Phys. Lett.*, vol. 76, no. 25, pp. 3804, 2000, doi: 10.1063/1.126787.

[75] C. Jiang, K. Kiyofumi, Y. Wang, and K. Koumoto, “Synthesis of BaTiO3. nanowires at low temperature,” *Cryst. Growth Des.*, vol. 7, no. 12, pp. 2713–2715, 2007, doi: 10.1021/cg0607607.

[76] Y. Wang *et al.*, “A general approach to porous crystalline TiO2, SrTiO 3, and BaTiO3 spheres,” *J. Phys. Chem. B*, vol. 110, no. 28, pp. 13835–13840, 2006, doi: 10.1021/jp061597t.

[77] K. Su, N. Nuraje, and N. L. Yang, “Open-bench method for the preparation of BaTiO 3, SrTiO 3, and Ba xSr 1-xTiO 3 nanocrystals at 80 °C,” *Langmuir*, vol. 23, no. 23, pp. 11369–11372, 2007, doi: 10.1021/la701877d.

[78] U. A. Joshi and J. S. Lee, “Template-free hydrothermal synthesis of single-crystalline barium titanate and strontium titanate nanowires,” *Small*, vol. 1, no. 12, pp. 1172–1176, 2005, doi: 10.1002/smll.200500055.

[79] Z. Deng, Y. Dai, W. Chen, X. Pei, and J. Liao, “Synthesis and characterization of bowl-like single-crystalline BaTiO 3 nanoparticles,” *Nanoscale Res. Lett.*, vol. 5, no. 7, pp. 1217–1221, 2010, doi: 10.1007/s11671-010-9629-7.

[80] M. M. Koebel, D. Y. Nadargi, G. Jimenez-Cadena, and Y. E. Romanyuk, “Transparent, conducting ATO thin films by epoxide-initiated solgel chemistry: A highly versatile route to mixed-metal oxide films,” *ACS Appl. Mater. Interfaces*, vol. 4, no. 5, pp. 2464–2473, 2012, doi: 10.1021/am300143z.

[81] L. Spanhel, “Colloidal ZnO nanostructures and functional coatings: A survey,” *J. Sol-Gel Sci. Technol.*, vol. 39, no. 1 SPEC. ISS., pp. 7–24, 2006, doi: 10.1007/s10971-006-7302-5.

[82] L. Znaidi, “Sol-gel-deposited ZnO thin films: A review,” *Mater. Sci. Eng. B Solid-State Mater. Adv. Technol.*, vol. 174, no. 1–3, pp. 18–30, 2010, doi: 10.1016/j.mseb.2010.07.001.

[83] O. Tari, A. Aronne, M. L. Addonizio, S. Daliento, E. Fanelli, and P. Pernice, “Sol-gel synthesis of ZnO transparent and conductive films: A critical approach,” *Sol. Energy Mater. Sol. Cells*, vol. 105, pp. 179–186, 2012, doi: 10.1016/j.solmat.2012.06.016.

[84] P. Sagar, P. K. Shishodia, and R. M. Mehra, “Influence of pH value on the quality of sol-gel derived ZnO films,” *Appl. Surf. Sci.*, vol. 253, no. 12, pp. 5419–5424, 2007, doi: 10.1016/j.apsusc.2006.12.026.

[85] B. Houng, C. Lou Huang, and S. Y. Tsai, “Effect of the pH on the growth and properties of sol-gel derived boron-doped ZnO transparent conducting thin film,” *J. Cryst. Growth*, vol. 307, no. 2, pp. 328–333, 2007, doi: 10.1016/j.jcrysgro.2007.07.001.

[86] S. Ilican, F. Yakuphanoglu, M. Caglar, and Y. Caglar, “The role of pH and boron doping on the characteristics of sol gel derived ZnO films,” *J. Alloys Compd.*, vol. 509, no. 17, pp. 5290–5294, 2011, doi: 10.1016/j.jallcom.2011.01.122.

[87] W. Wang, L. Cao, W. Liu, G. Su, and W. Zhang, “Low-temperature synthesis of BaTiO3 powders by the sol-gel-hydrothermal method,” *Ceram. Int.*, vol. 39, no. 6, pp. 7127–7134, 2013, doi: 10.1016/j.ceramint.2013.02.055.

[88] B. Robertz, F. Boschini, R. Cloots, and A. Rulmont, “Importance of soft solution processing for advanced BaZrO3 materials,” *Int. J. Inorg. Mater.*, vol. 3, no. 8, pp. 1185–1187, 2001, doi: 10.1016/S1466-6049(01)00122-2.

[89] X. Zhang *et al.*, “Synthesis of cadmium titanate powders by a sol-gel-hydrothermal method,” *J. Mater. Sci.*, vol. 38, no. 11, pp. 2353–2356, 2003, doi: 10.1023/A:1023932513481.

[90] Q. Chang, J. E. Zhou, Y. Wang, and G. Meng, “Formation mechanism of zirconia nano-particles containing pores prepared via sol-gel-hydrothermal method,” *Adv. Powder Technol.*, vol. 21, no. 4, pp. 425–430, 2010, doi: 10.1016/j.apt.2009.11.003.

[91] Z. Chen, J. Hu, Z. Lu, and X. He, “Low-temperature preparation of lanthanum-doped BiFeO3 crystallites by a sol-gel-hydrothermal method,” *Ceram. Int.*, vol. 37, no. 7, pp. 2359–2364, 2011, doi: 10.1016/j.ceramint.2011.03.081.

[92] L. Hou, Y. D. Hou, X. M. Song, M. K. Zhu, H. Wang, and H. Yan, “Sol-gel-hydrothermal synthesis and sintering of K0.5Bi0.5TiO3 nanowires,” *Mater. Res. Bull.*, vol. 41, no. 7, pp. 1330–1336, 2006, doi: 10.1016/j.materresbull.2005.12.010.

[93] F. Yu, J. Yang, J. Ma, J. Du, and Y. Zhou, “Preparation of nanosized CoAl2O4 powders by sol-gel and sol-gel-hydrothermal methods,” *J. Alloys Compd.*, vol. 468, no. 1–2, pp. 443–446, 2009, doi: 10.1016/j.jallcom.2008.01.018.

[94] Y. D. Hou, L. Hou, J. L. Zhao, M. K. Zhu, and H. Yan, “Lead-free Bi-based complex perovskite nanowires: Sol-gelhydrothermal processing and the densification behavior,” *J. Electroceramics*, vol. 26, no. 1–4, pp. 37–43, 2011, doi: 10.1007/s10832-010-9625-4.

[95] H. Liu, P. Zhou, L. Zhang, Z. Liang, H. Zhao, and Z. Wang, “Effects of oxygen partial pressure on the structural and optical properties of undoped and Cu-doped ZnO thin films prepared by magnetron co-sputtering,” *Mater. Lett.*, vol. 164, pp. 509–512, 2016, doi: 10.1016/j.matlet.2015.11.038.

[96] A. I. Ali, A. H. Ammar, and A. Abdel Moez, “Influence of substrate temperature on structural, optical properties and dielectric results of nano- ZnO thin films prepared by Radio Frequency technique,” *Superlattices Microstruct.*, vol. 65, pp. 285–298, 2014, doi: 10.1016/j.spmi.2013.11.007.

[97] T. K. Pathak, V. Kumar, H. C. Swart, and L. P. Purohit, “Electrical and optical properties of p-type codoped ZnO thin films prepared by spin coating technique,” *Phys. E Low-Dimensional Syst. Nanostructures*, vol. 77, pp. 1–6, 2016, doi: 10.1016/j.physe.2015.11.001.

[98] A. Mortezaali, O. Taheri, and Z. S. Hosseini, “Thickness effect of

nanostructured ZnO thin films prepared by spray method on structural, morphological and optical properties," *Microelectron. Eng.*, vol. 151, pp. 19–23, 2016, doi: 10.1016/j.mee.2015.11.016.

[99] Y. Mao, S. Banerjee, and S. S. Wong, "Hydrothermal synthesis of perovskite nanotubes," *Chem. Commun.*, vol. 9, no. 3, pp. 408–409, 2003, doi: 10.1039/b210633g.

[100] A. A. El Mel, R. Nakamura, and C. Bittencourt, "The Kirkendall effect and nanoscience: Hollow nanospheres and nanotubes," *Beilstein J. Nanotechnol.*, vol. 6, no. 1, pp. 1348–1361, 2015, doi: 10.3762/bjnano.6.139.

[101] X. Huang, B. Sun, Y. Zhu, S. Li, and P. Jiang, "High-k polymer nanocomposites with 1D filler for dielectric and energy storage applications," *Prog. Mater. Sci.*, vol. 100, no. September 2018, pp. 187–225, 2019, doi: 10.1016/j.pmatsci.2018.10.003.

[102] M. Rahimabady, M. S. Mirshekarloo, K. Yao, and L. Lu, "Dielectric behaviors and high energy storage density of nanocomposites with core–shell BaTiO3@TiO2 in poly(vinylidene fluoride-hexafluoropropylene)," *Phys. Chem. Chem. Phys.*, vol. 15, no. 38, pp. 16242–16248, 2013.

[103] K. Bi *et al.*, "Ultrafine core-shell BaTiO3@SiO2 structures for nanocomposite capacitors with high energy density," *Nano Energy*, vol. 51, no. July, pp. 513–523, 2018, doi: 10.1016/j.nanoen.2018.07.006.

[104] H. Luo *et al.*, "Interface design for high energy density polymer nanocomposites," *Chem. Soc. Rev.*, vol. 48, no. 16, pp. 4424–4465, 2019, doi: 10.1039/c9cs00043g.

[105] J. P. Calame, "Finite difference simulations of permittivity and electric field statistics in ceramic-polymer composites for capacitor applications," *J. Appl. Phys.*, vol. 99, no. 8, 2006, doi: 10.1063/1.2188032.

[106] B. Ates, S. Koytepe, A. Ulu, C. Gurses, V.K. Thakur, "Chemistry, Structures, and Advanced Applications of Nanocomposites from Biorenewable Resources" Chemical Reviews (2020), 10.1021/acs.chemrev.9b00553

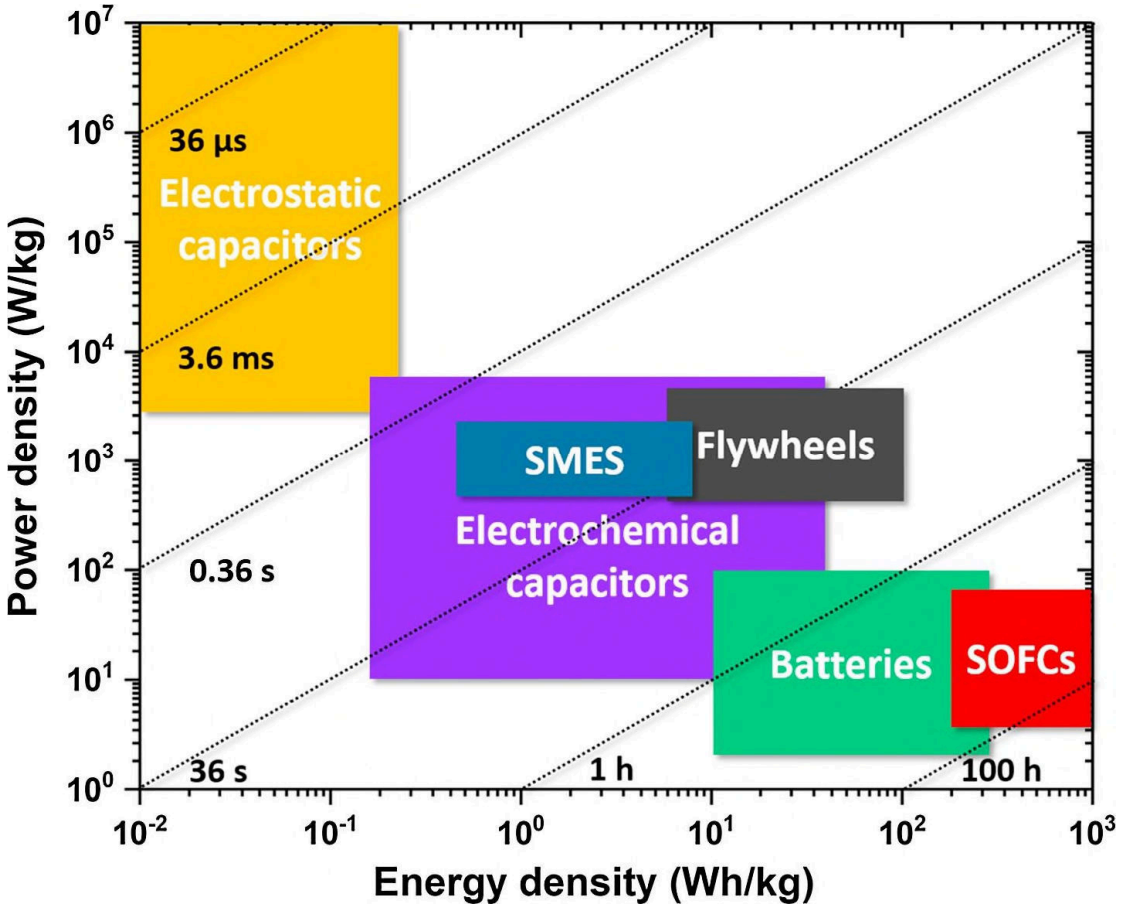

Figure 1: Specific power against specific energy of different electrical devices. Reprinted with permission from Ref. [2]

Figure 2: Diverse application fields of capacitors Reprinted with permission from Ref. [2]

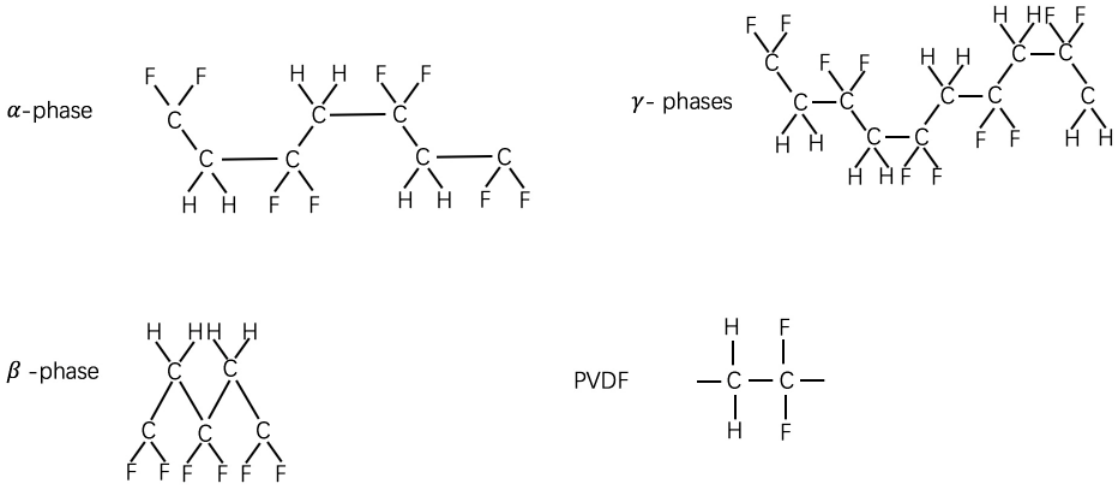

Figure 3: The α, β, γ phases of PVDF and common PVDF structure. Adapted from ref [14].

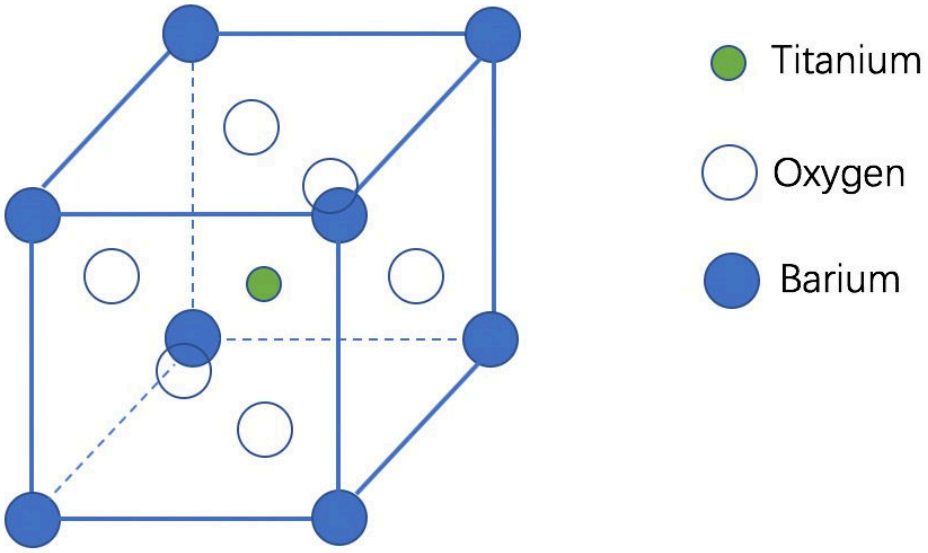

Figure 4: The structure of Barium Titanium Oxide.

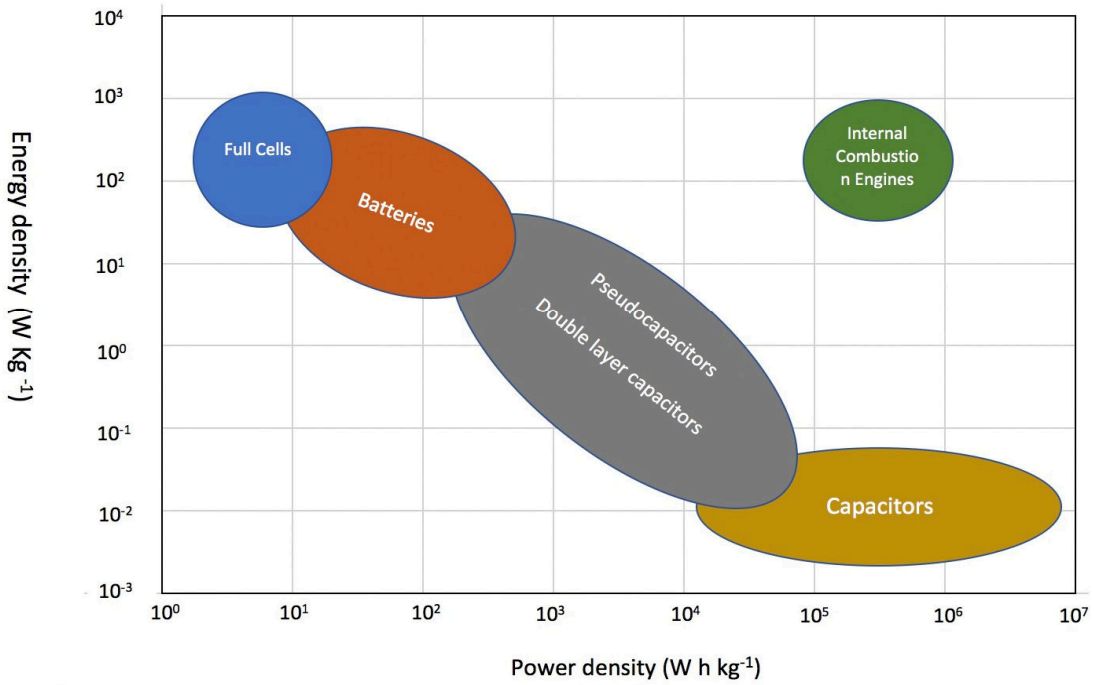

Figure 5: The energy storage ability of different electric energy storage devices. Reprinted with permission from Ref. [46].

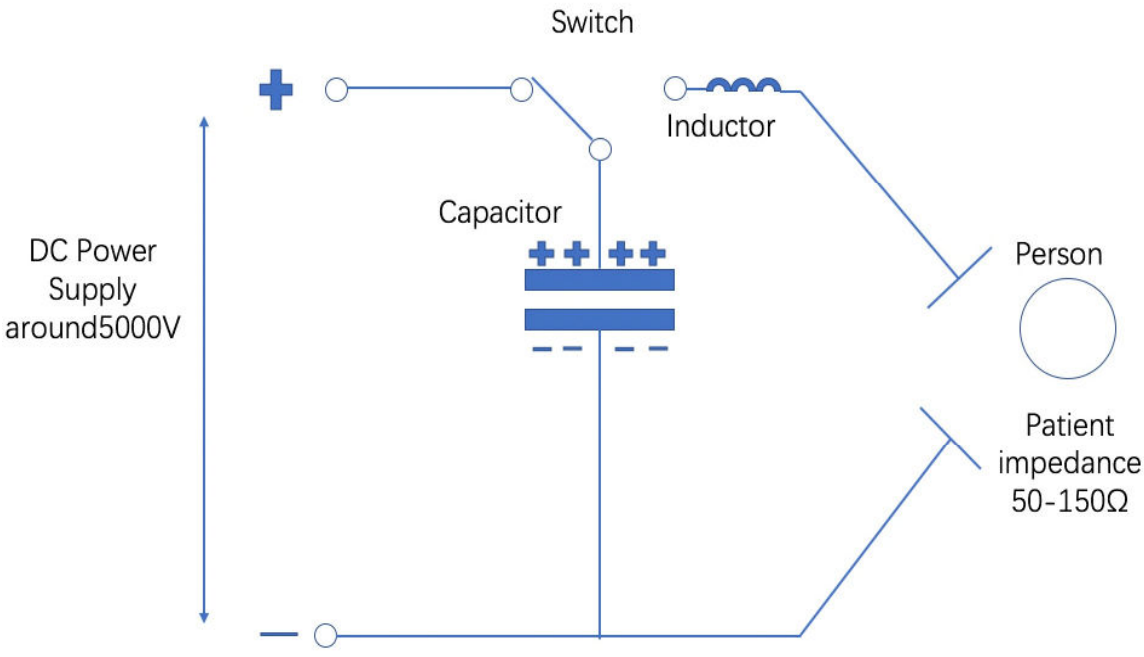

Figure 6: Simplified schematic of defibrillators. Reprinted with permission from Ref. [50].

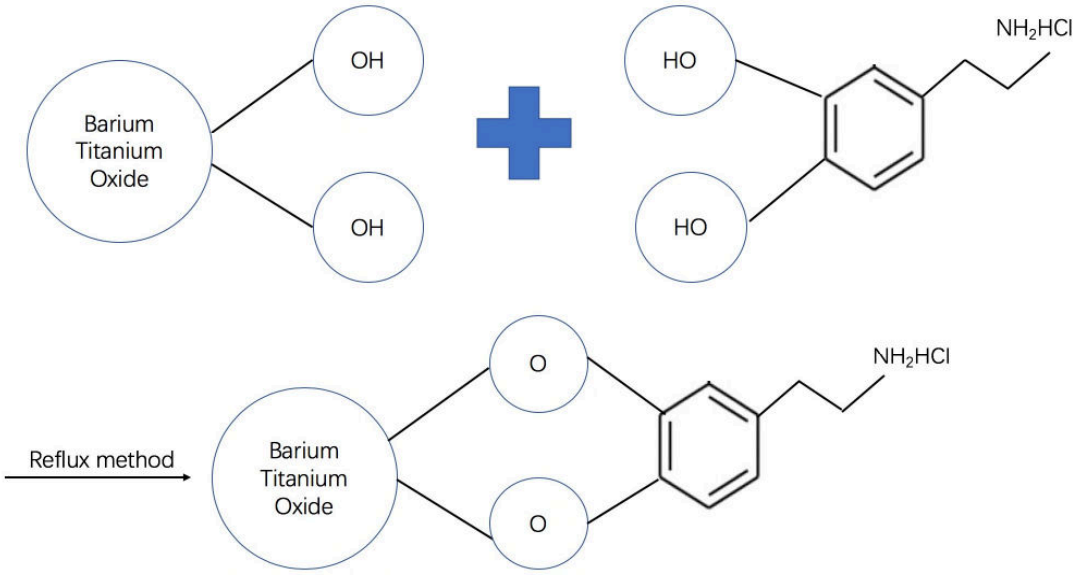

Figure 7: The scheme for dopamine surface functionalized $BaTiO_3$. Reproduced with permission from Ref. [12].

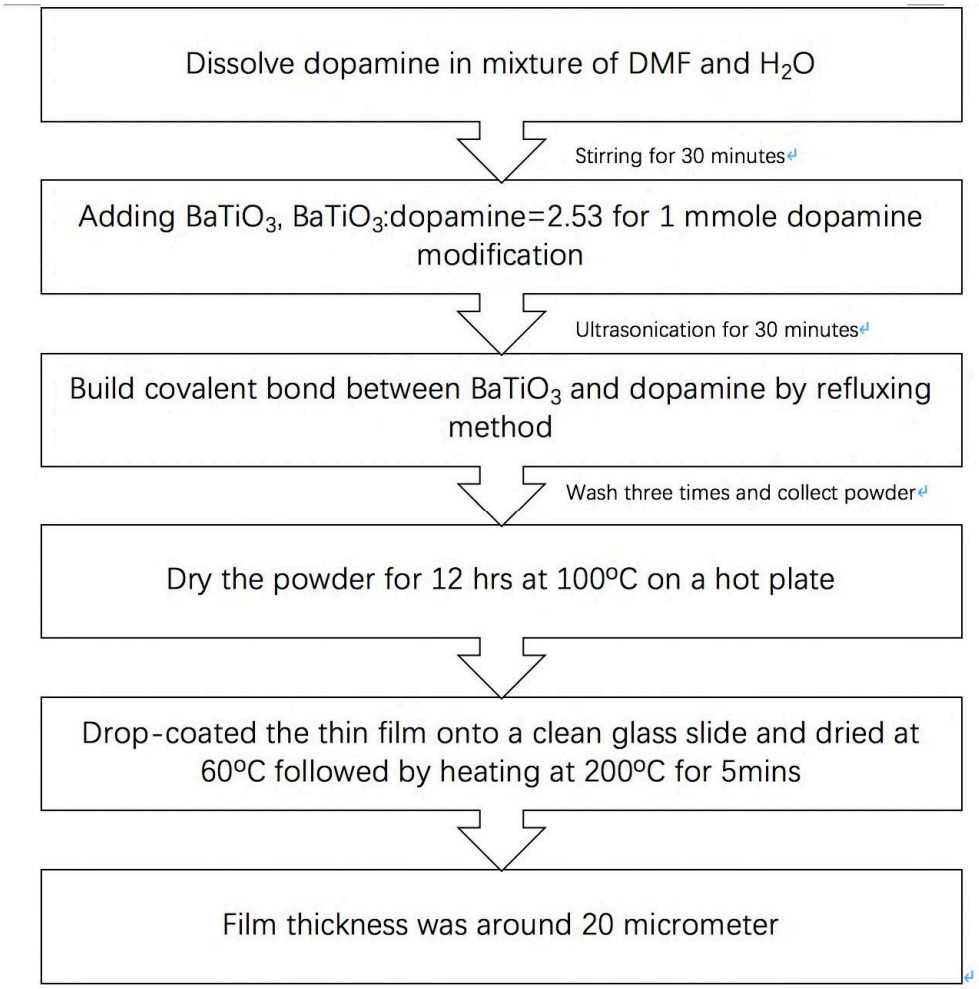

Figure 8: The process of functionalize the $BaTiO_3$ with dopamine by hydrothermal method.

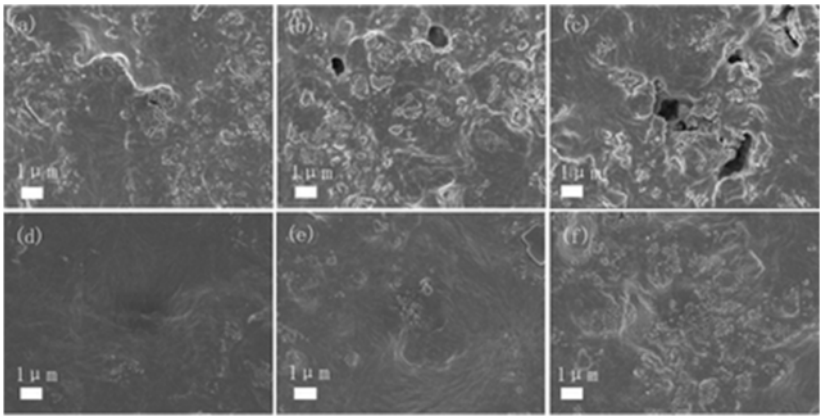

Figure 9: FE-SEM images of $BaTiO_3$/PVDF thin film composites with various weight% of $BaTiO_3$: (a) 10%, (b) 30%, (c) 50% without dopamine; and (d) 10%, (e) 30%, (f) 50% with dopamine. Reprinted with permission from Ref. [12].

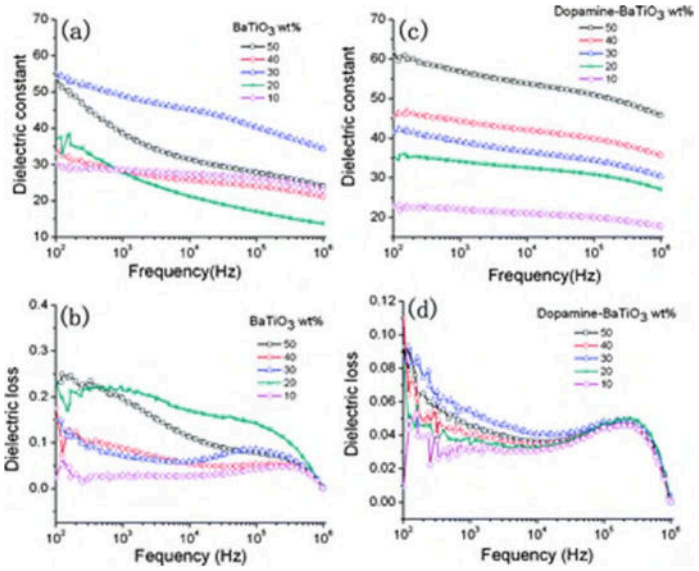

Figure 10: Dependences of (a) dielectric constant and (b) dielectric loss of $BaTiO_3$/PVDF composites; (c) dielectric constant and (d) dielectric loss of dopamine–$BaTiO_3$/PVDF composites on frequency measured at room temperature from 10^2 to 10^6 Hz. Reprinted with permission from Ref. [12].

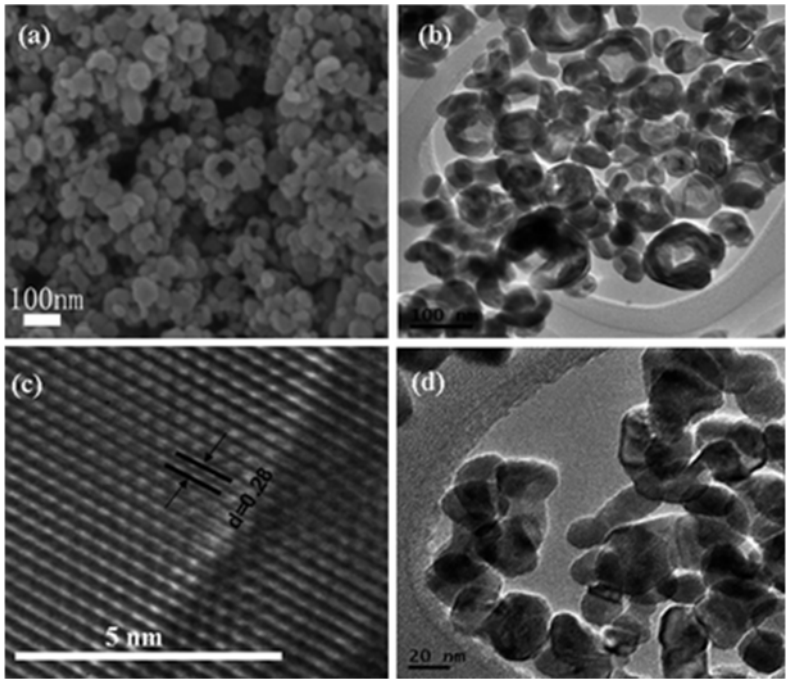

Figure 11: (a) The FESEM image of hollow 10 at% Nd_2O_3–$BaTiO_3$nanoparticle at 200 °C/2 h. (b) The TEM image of 10 at% Nd_2O_3–$BaTiO_3$nanoparticle at 200 °C/2 h. (c) The HR-TEM image of a single tetragonal hollow 10 at% Nd_2O_3–$BaTiO_3$nanoparticle. (d) The TEM image of $BaTiO_3$nanoparticle at 200 °C/2 h. Reprinted with permission from Ref. [47].

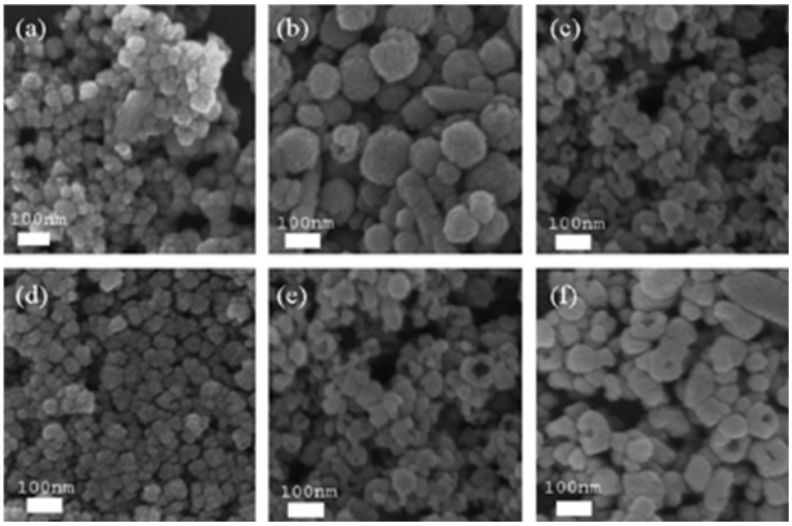

Figure 12: Fe-SEM images of a doped $BaTiO_3$ hollow structure synthesized for 2 h at (a) 120 °C, (b) 160 °C and (c) 200 °C; synthesized at 200 °C for (d) 0.5 h, (e) 2 h and (f) 24 h Reprinted with permission from Ref. [64].

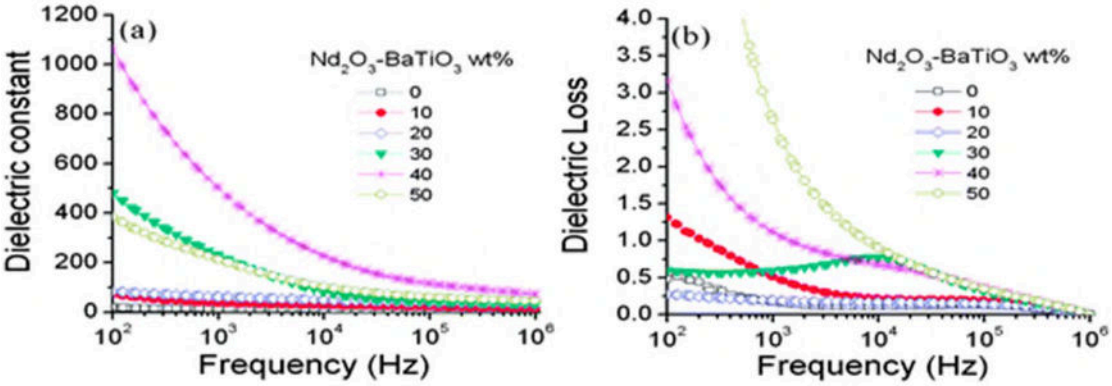

Figure 13: Dependences of (a) dielectric constant and (b) dielectric loss of 10 at% Nd_2O_3–$BaTiO_3$/PVDF composites on frequency measured at room temperature from 10^2 to 10^6 Hz, respectively. Reprinted with permission from Ref. [64].

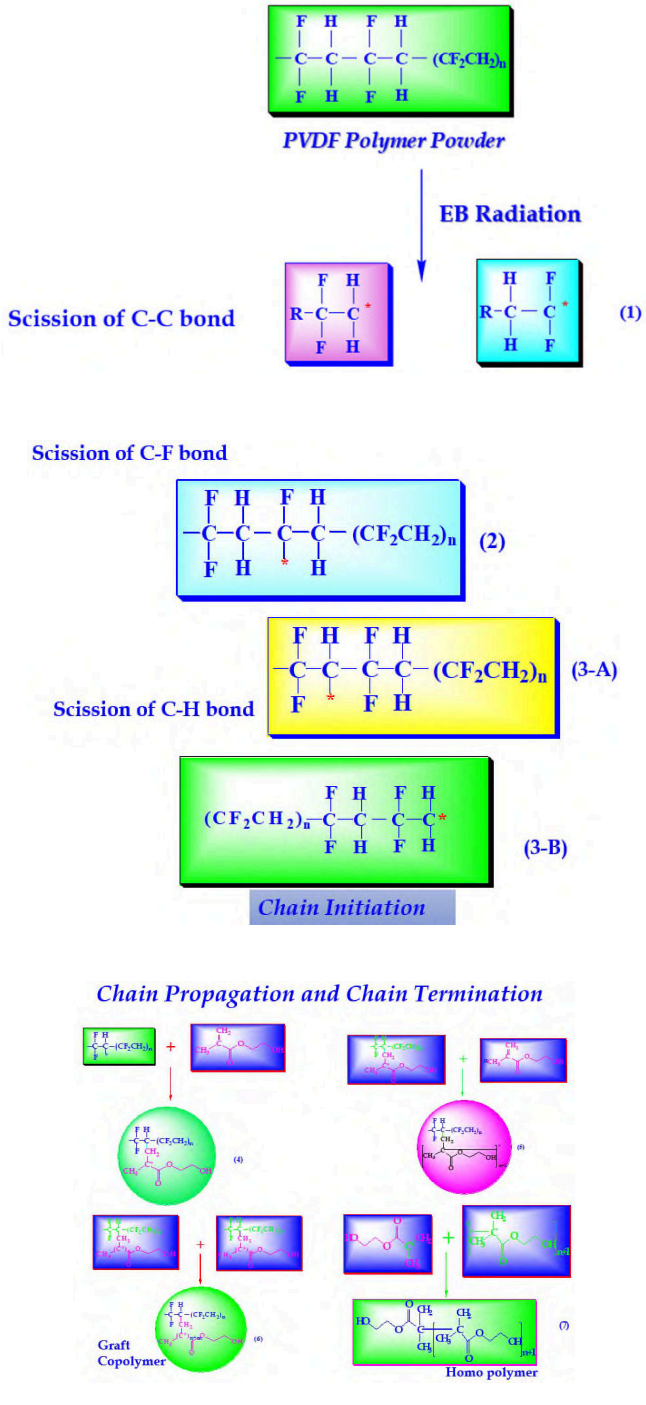

Figure 14: Mechanism for graft copolymerization of HEMA onto pristine PVDF polymer Reprinted with permission from Ref. [10].

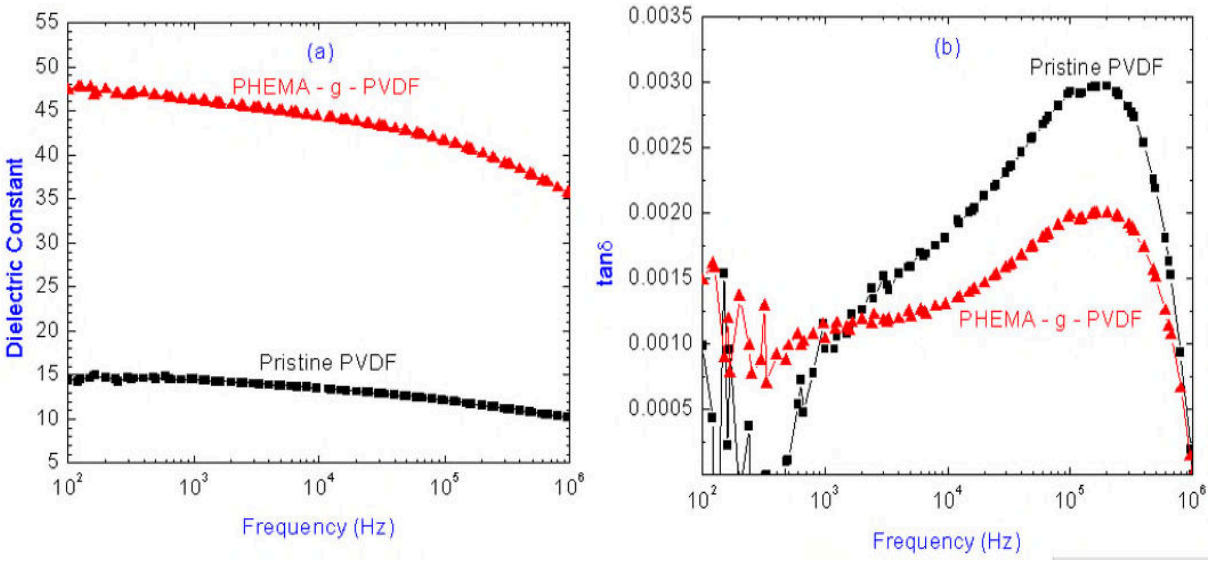

Figure 15: Dielectric Properties of PVDF-g-HEMA [8]. Reprinted with permission from Ref. [10]. (a) The dielectirc constant of pristine PVDF and PHEMA grafted PVDF. (b) The dielectric loss of pristine PVDF and PHEMA grafted PVDF.

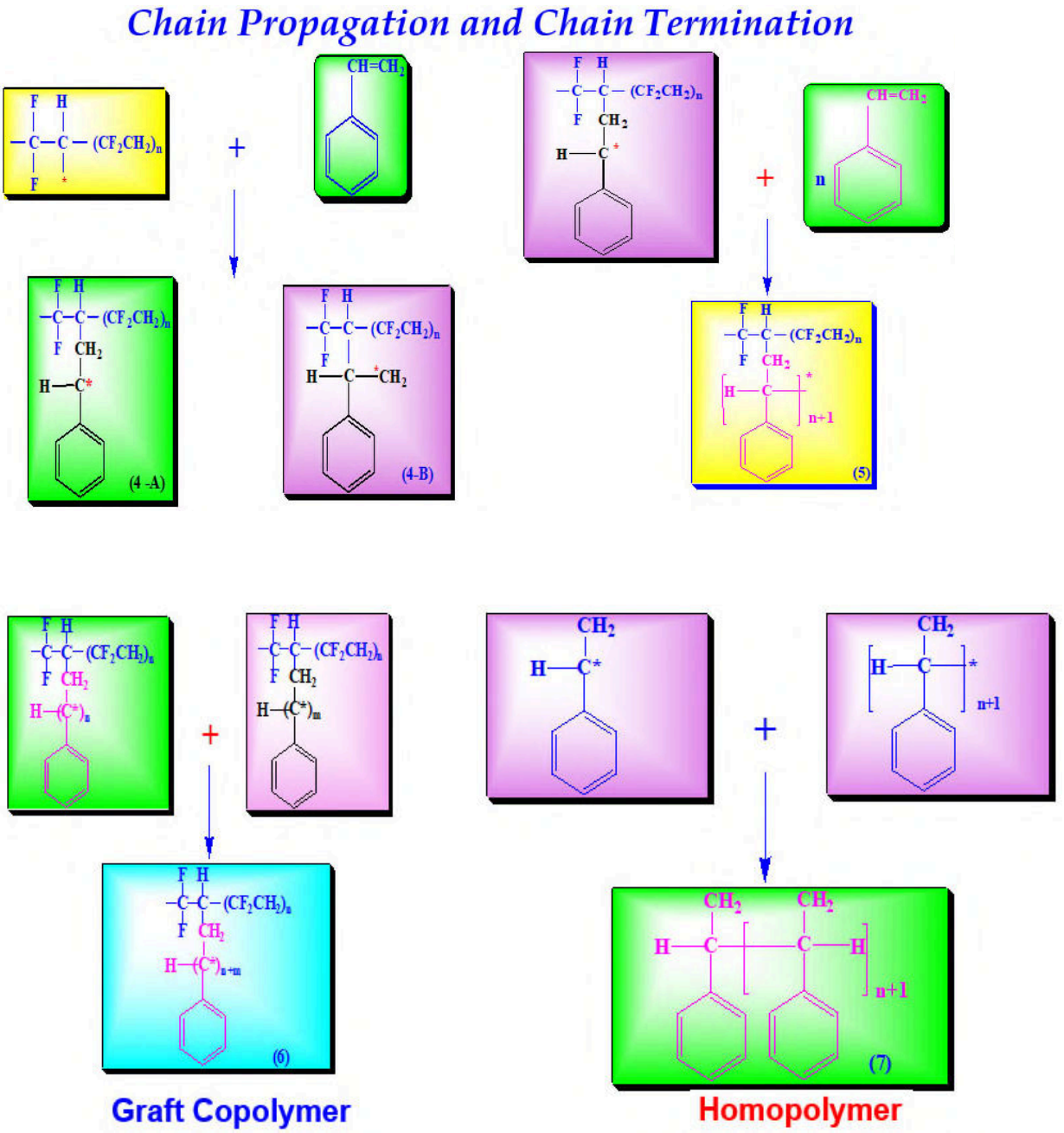

Figure 16 Mechanism for graft copolymerization of styrene onto pristine PVDF polymer [11]. Reprinted with permission from Ref. [11].

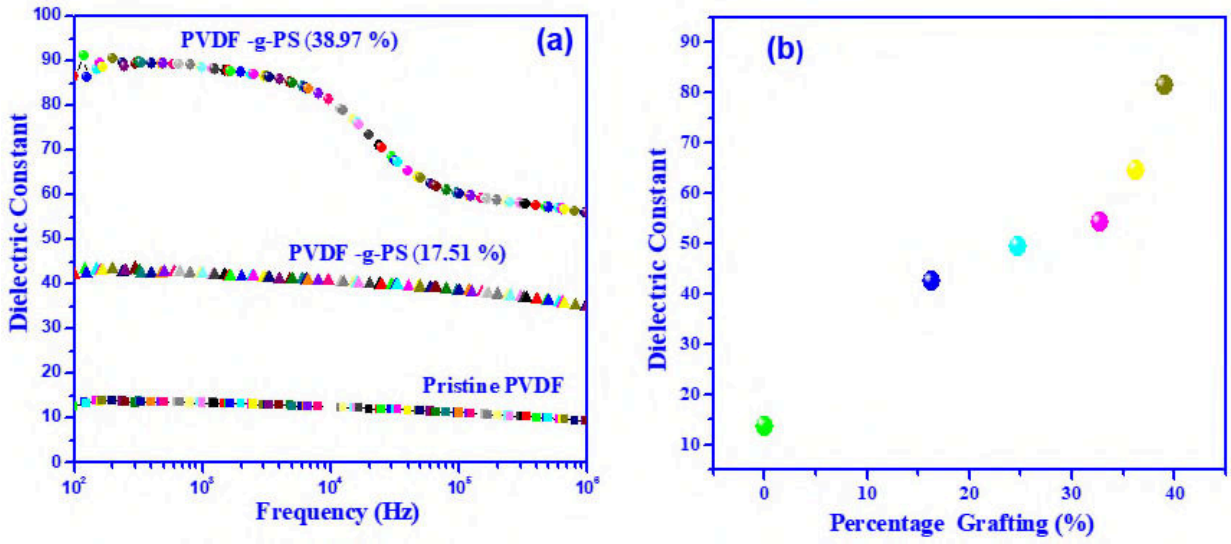

Figure 17 (a) Dependence of the dielectric constant on various frequencies at room temperature for pristine PVDF, optimum (38.97%) and lowest grafted PVDF-*g*-PS (17.51%) polymer films. (b) Effect of the percentage of grafting of PS onto the dielectric constant of PVDF at room temperature measured at 100 Hz. Reprinted with permission from Ref. [11].

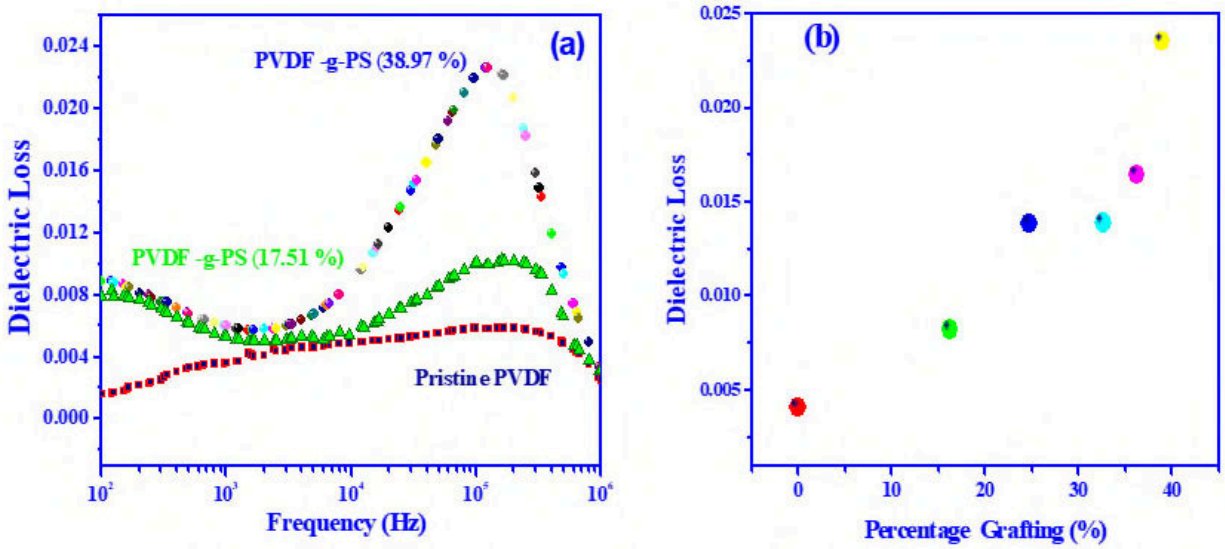

Figure 18 (a) Dependence of dielectric losses on the frequency at room temperature. (b) Effect of the percentage of grafting of PS onto the PVDF at room temperature measured at 100 Hz. Reprinted with permission from Ref. [11].

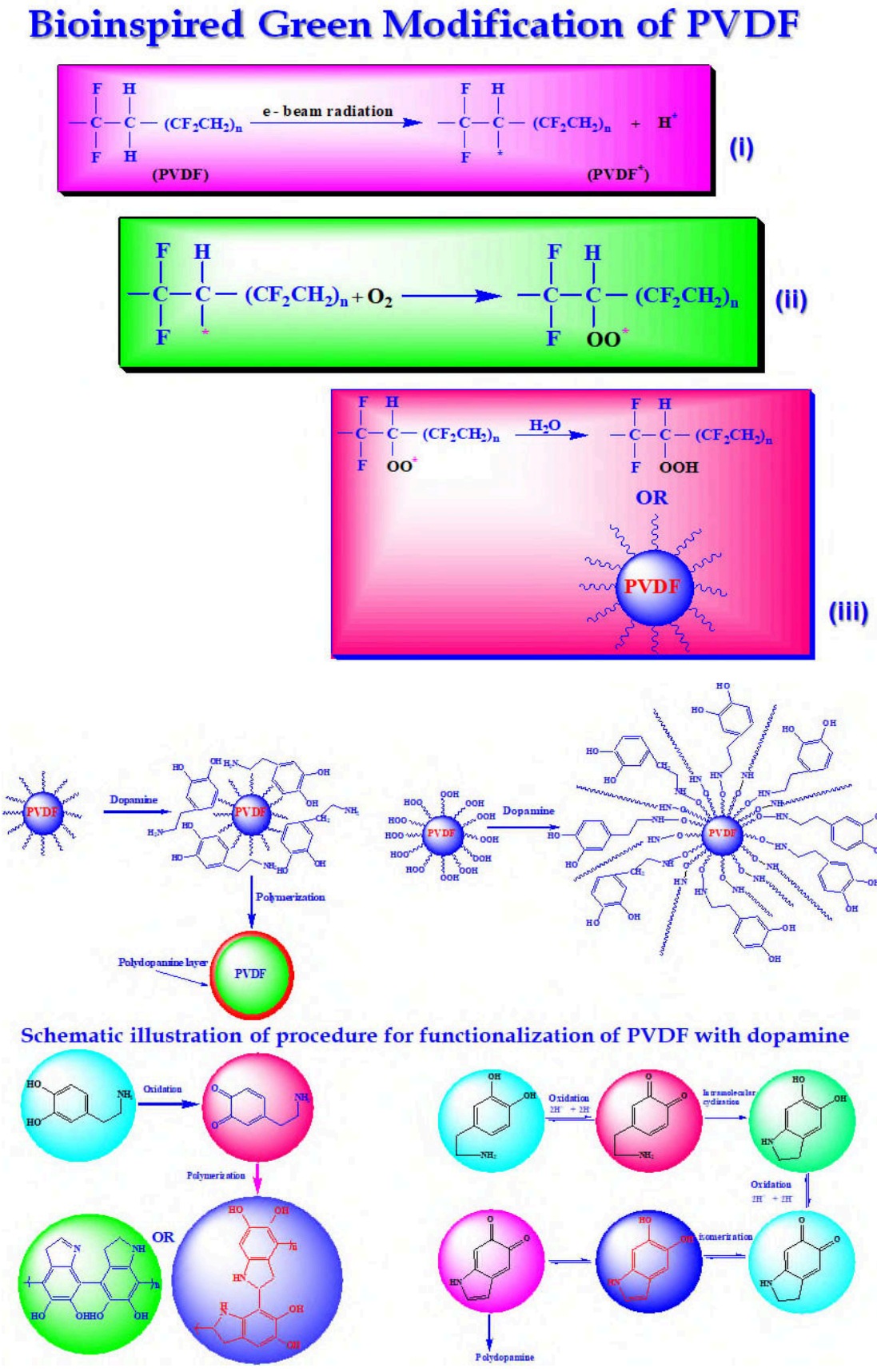

Figure 19: Bioinspired surface modification of PVDF. Reprinted with permission from Ref. [3].

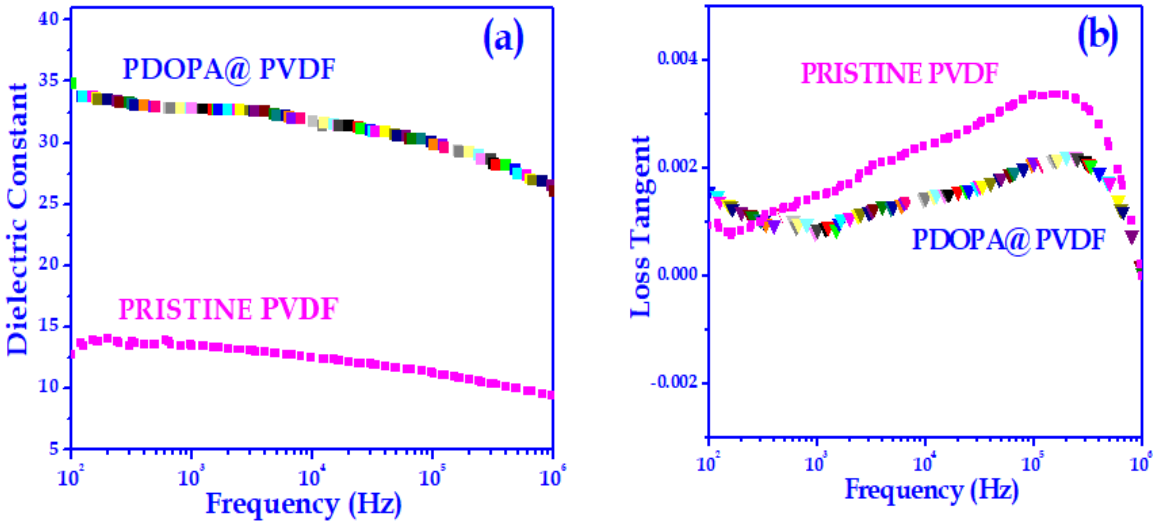

Figure 20: Dielctric properties of the pristine nad surface modified PVDF. (a) Dependence of the dielectric constant of pristine PVDF and modified PVDF, (b) The dielectric loss on frequency at room temperature of pristine PVDF and modified PVDF. Reprinted with permission from Ref. [3]

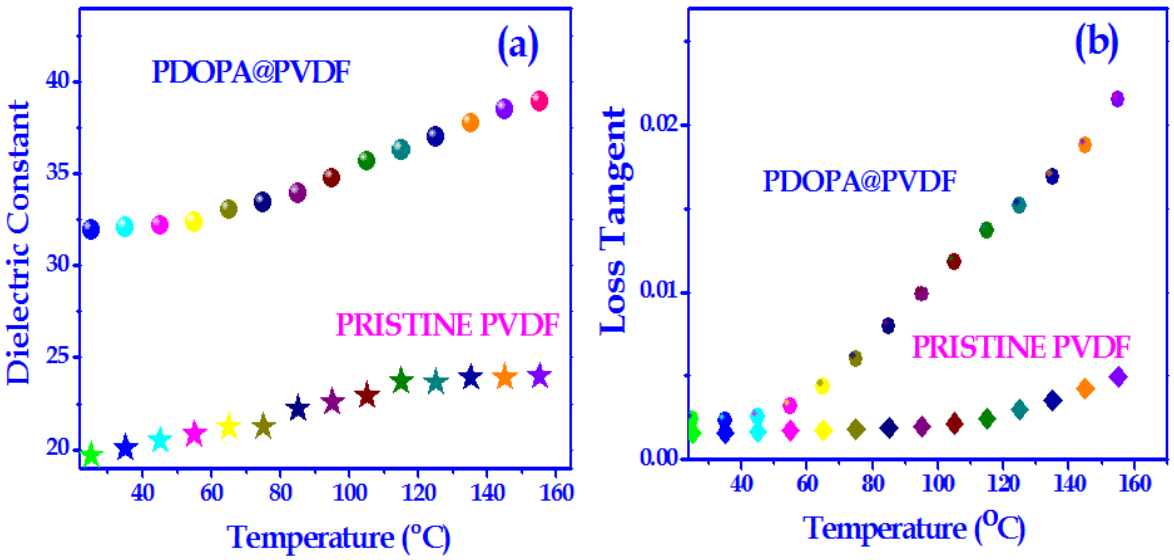

Figure 21: Effect of temperature on the dielectric properties of the pristine and surface modified PVDF. (a) Dependence of the dielectric constant of POOPA@PVDF and PVDF (b) The dielectric losses on temperature at the frequency of 10kHz of POOPA@PVDF and PVDF. Reprinted with permission from Ref. [3].

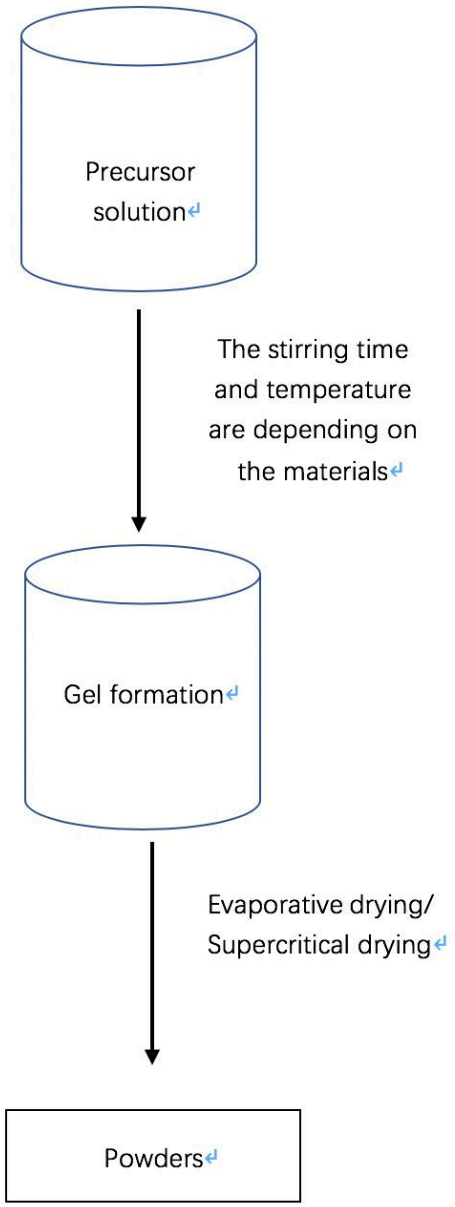

Figure 22: Simplify process of sol-gel.

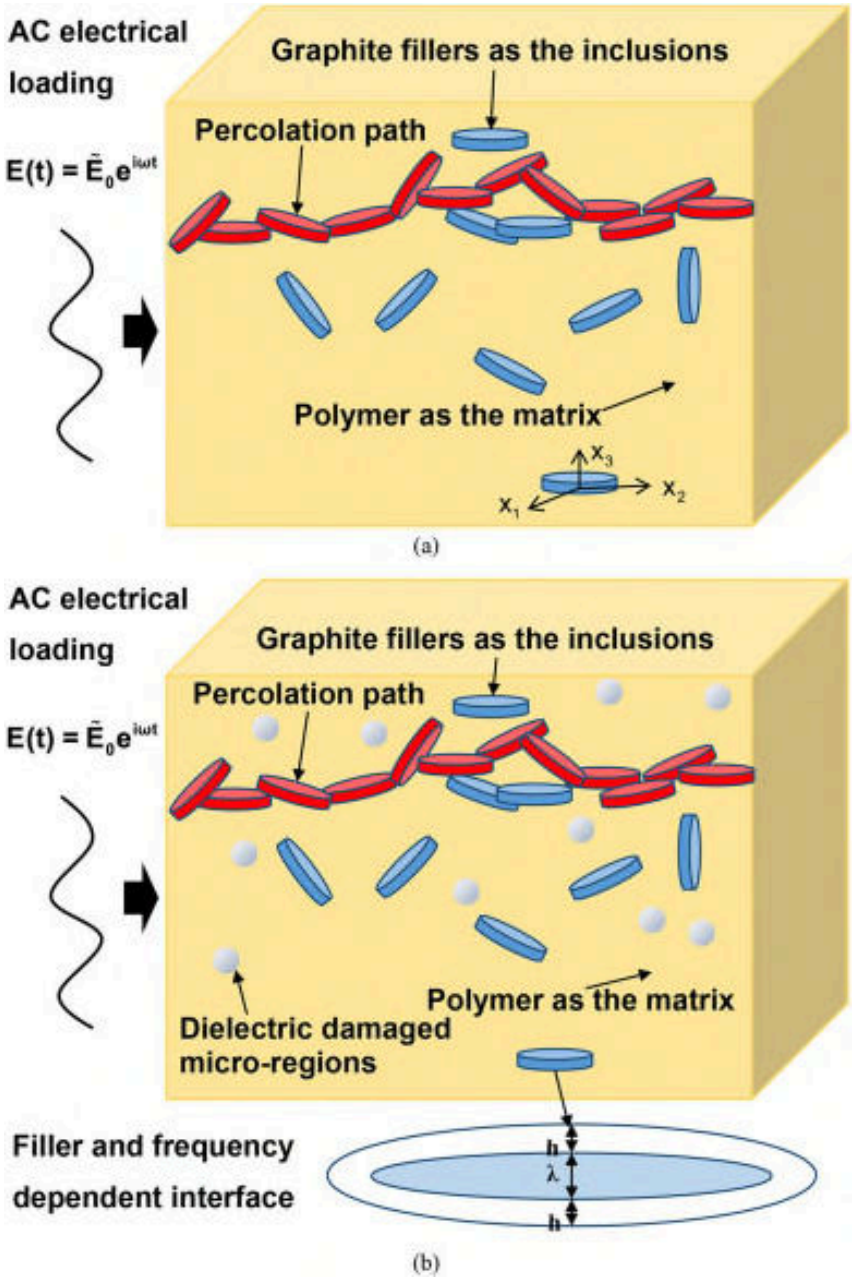

Figure 23: Dielectric properties of graphite composite**.** (a)Before dielectric damage process, (b) the loss of dielectric permittivity. Reprinted with permission from Ref. [65].

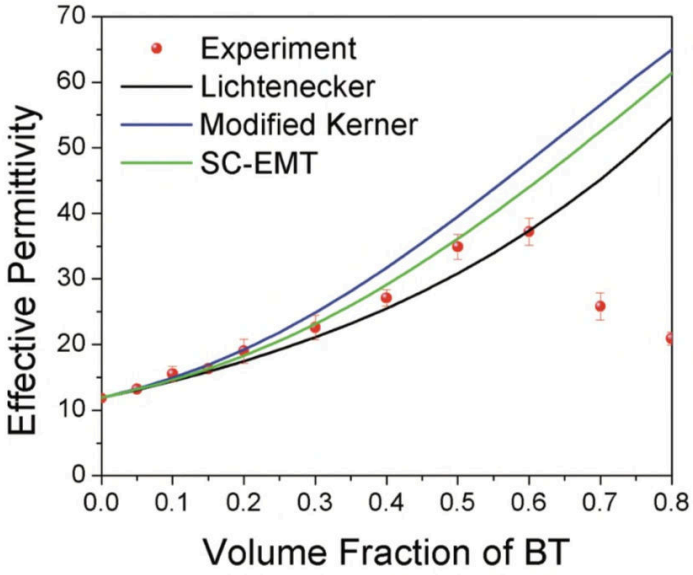

Figure 24: Comparison of experimental effective permittivity at different volume fraction of BTO with calculated results from different models. Reprinted with permission from Ref. [7]

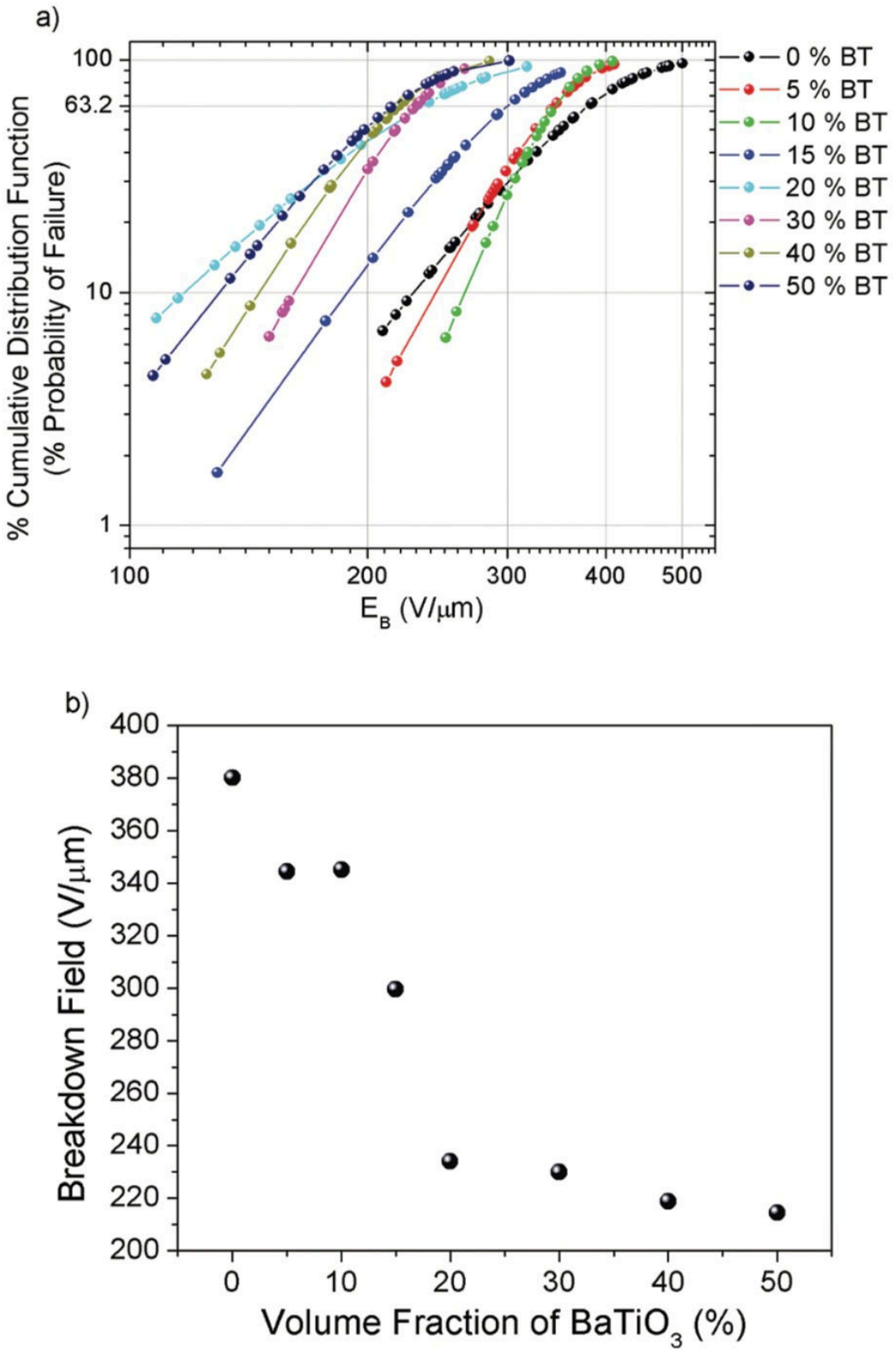

Figure 25: (a) The probability of failure of nanocomposites with different volume fraction of BTO and (b) the breakdown strength nanocomposite with different volume fraction when the probability of failure is 63.2%. Reprinted with permission from Ref. [7]

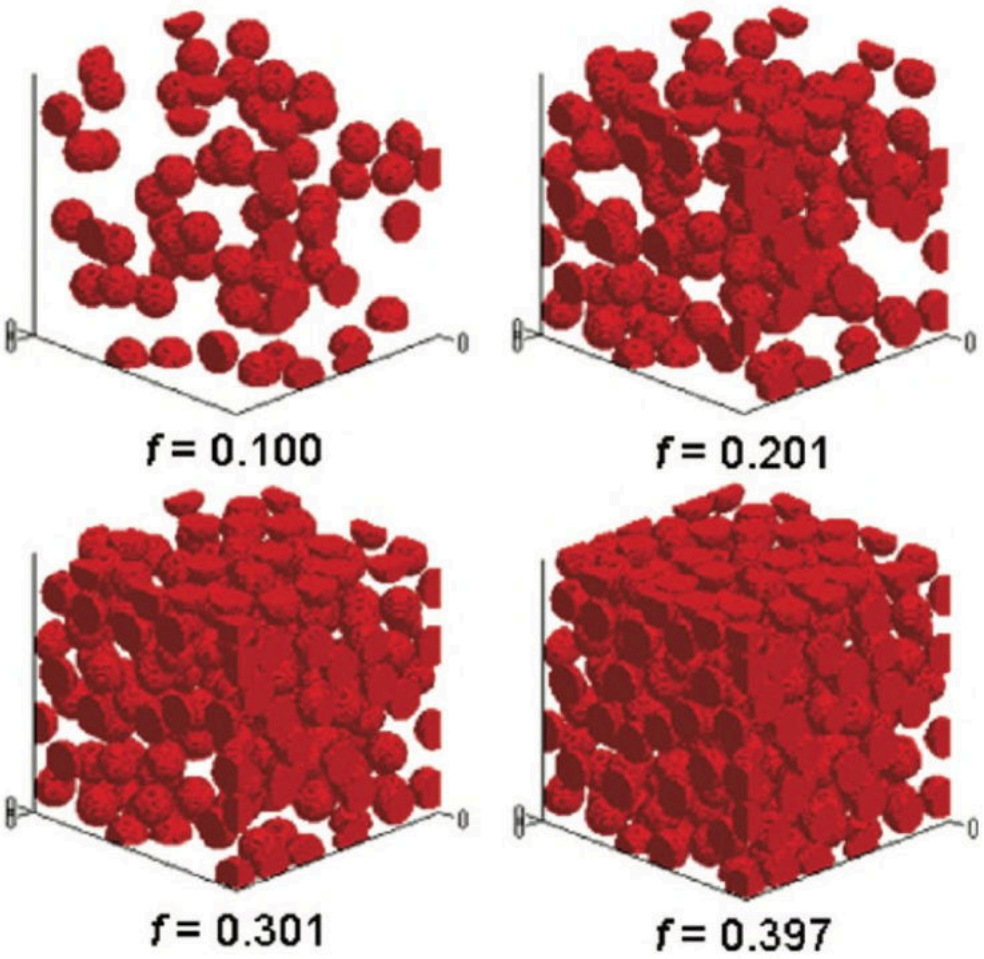

Figure 26: Example of how the Cellular packing model simulate the status of particles at different volume fraction. Reprinted with permission from Ref. [7]

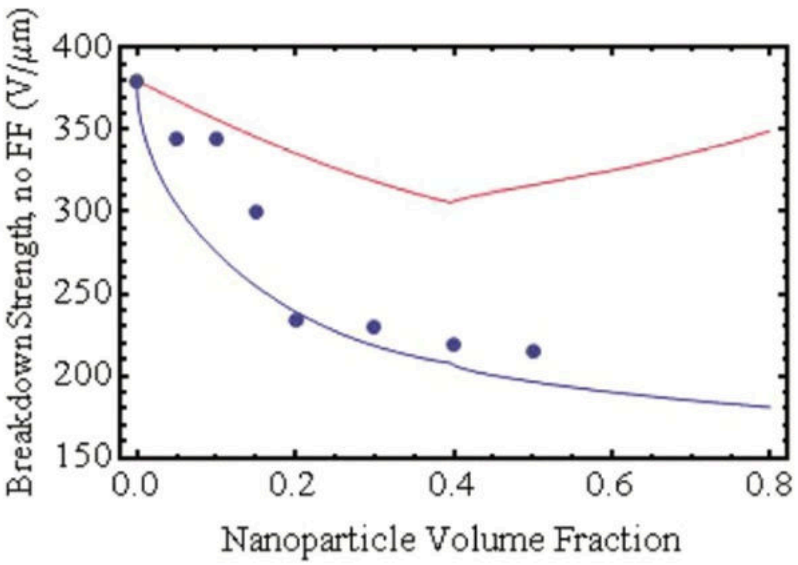

Figure 27: The breakdown strength calculated by different simulations (lines) and experimental values (dots). Reprinted with permission from Ref. [7]

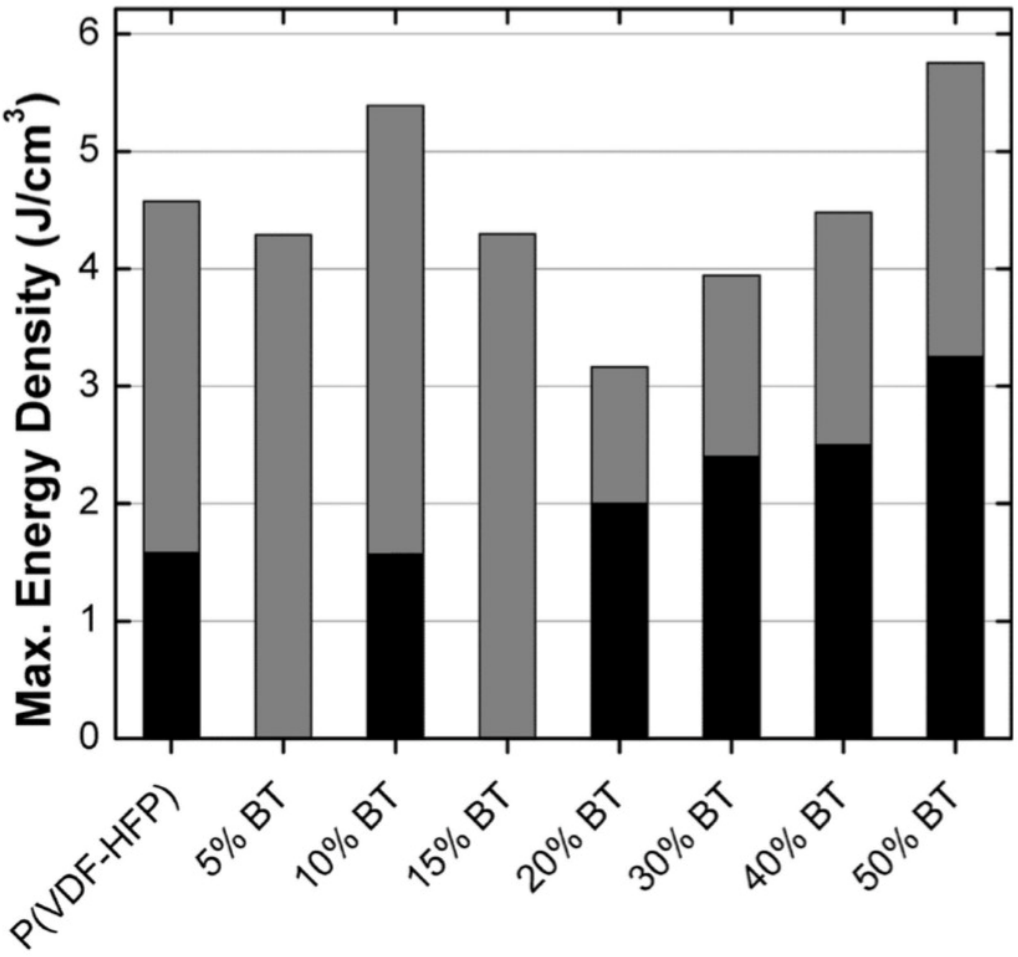

Figure 28: The calculated maximum energy density of nanocomposite with differnte volume fraction (black) and predicted maximum energy density of nanocomposite with different volume fraction (grey). Reprinted with permission from Ref. [7]

Table 1: Summary of nanocomposites with enhanced dielectric properties, modifications applied, and the main influence effect factors.

Nanocomposite	Modification	Main factors
Graphene/ZnO [17-18] PVDF/ZnO [15-16] PVDF/TiO_2 [17]	Doping [13,15,17-18]	Amount of dopant/volume fraction [7]
PVDF-HFP/ZnO/TiO_2 [15] PS-PVDF [11] PVDF-TrFE [82]	Co-polymer [11,15] Pre-irradiated PVDF [3]	Irradiation [11] – Dose intensity – Reaction time – Reaction temperature – Monomer concentration Solvent [11, 67]
PVDF/$BaTiO_3$ [35-36, 56-57] PVDF/$BaTiO_3$-Nd_2O_3 [63]	Surface modification: – Phosphoic acid [56-57] – Ethylene diamine [56-57] – Dopamine [12, 61] – Phosphate esters [54-55] – Oligomers [54-55]	Matrix-filler interface [61-62, 56-57]
Al-ZnO [67,83]	Control the pH value [67]	pH value [67,83] – TEA [83] – ZAD [83] – Acetic acid [83] – MEA [84] – Glacial acetic [85-86] – Ammonia [85-86]